



OPEN ACCESS

EDITED BY
Teemu Hölttä,
University of Helsinki, Finland

REVIEWED BY
Jarmila Pittermann,
University of California, Santa Cruz,
United States
Uwe Hacke,
University of Alberta, Canada

*CORRESPONDENCE
William J. Mattheaus
willmatt@udel.edu

†These authors have contributed
equally to this work and share last
authorship

SPECIALTY SECTION
This article was submitted to
Paleoecology,
a section of the journal
Frontiers in Ecology and Evolution

RECEIVED 28 May 2022
ACCEPTED 23 August 2022
PUBLISHED 12 September 2022

CITATION
Mattheaus WJ, Montañez IP,
McElwain JC, Wilson JP and White JD
(2022) Stems matter: Xylem
physiological limits are an accessible
and critical improvement to models
of plant gas exchange in deep time.
Front. Ecol. Evol. 10:955066.
doi: 10.3389/fevo.2022.955066

COPYRIGHT
© 2022 Mattheaus, Montañez,
McElwain, Wilson and White. This is an
open-access article distributed under
the terms of the [Creative Commons
Attribution License \(CC BY\)](https://creativecommons.org/licenses/by/4.0/). The use,
distribution or reproduction in other
forums is permitted, provided the
original author(s) and the copyright
owner(s) are credited and that the
original publication in this journal is
cited, in accordance with accepted
academic practice. No use, distribution
or reproduction is permitted which
does not comply with these terms.

Stems matter: Xylem physiological limits are an accessible and critical improvement to models of plant gas exchange in deep time

William J. Mattheaus^{1*}, Isabel P. Montañez¹,
Jennifer C. McElwain², Jonathan P. Wilson^{3†} and
Joseph D. White^{4†}

¹John Muir Institute of the Environment, University of California, Davis, Davis, CA, United States, ²Department of Botany, Trinity College Dublin, Dublin, Ireland, ³Department of Environmental Studies, Haverford College, Haverford, PA, United States, ⁴Department of Biology, Baylor University, Waco, TX, United States

The evolution of woody stems approximately 400 mya (middle Paleozoic) facilitated the expansion of plants and has likely affected carbon and water budgets across much of the terrestrial surface since that time. Stems are a carbon cost/sink and limit water transport from soil to leaves as it must pass through specialized xylem tissue. While leaf fossils have provided a wealth of quantitative data, including estimates of plant water fluxes utilizing biophysically based models, fossil-informed models integrating stem and leaf physiology are lacking. Integrated stem-leaf physiology may distinguish successors to ecological catastrophes like the end of the Late Paleozoic Ice Age (LPIA). The documented collapse of LPIA tropical forests provides an opportunity to assess the importance of woody stems as a key to understanding differences in survivorship among common plant taxa from the Carboniferous to the Permian. Here, we present an analysis of the limits to leaf water supply and plant function for Paleozoic forest plant types due to (1) cavitation-induced embolism and xylem blockage and (2) insufficient sapwood water transport capacity.—collectively defined here as sapwood dysfunction. We first present a modified ecosystem process model (*Paleo-BGC+*) that includes sapwood dysfunction. *Paleo-BGC+* is parameterized using measurements obtainable from fossil xylem and therefore applicable to both modern and ancient ecosystems. We then assess the effect of sapwood dysfunction on ecosystem processes based on previously published fossil leaf measurements and a new fossil xylem dataset for plant types present in the Late Paleozoic. Using daily meteorology from a GCM of the late Carboniferous (GENESIS v3) under a Glacial (low-CO₂) and an Inter-glacial (high-CO₂) scenario, we found that simulated sapwood dysfunction slowed plant water use and reduced carbon storage. This inhibition occurred particularly in plants with high maximum stomatal conductance and high stem vulnerability

to embolism. Coincidentally, plants with these traits were predominantly reduced or missing from the fossil record from the Carboniferous to the Permian. Integrating stem and leaf physiology may improve the fidelity of model representations of soil-to-atmosphere water transport through plants, simulations of long-term climate phenomena like the LPIA, and ecosystem projections under future climate change.

KEYWORDS

sapwood, stomatal conductance (g_s), ecosystem process and function, ecosystem process model, fossils, xylem, cavitation-induced embolism

Introduction

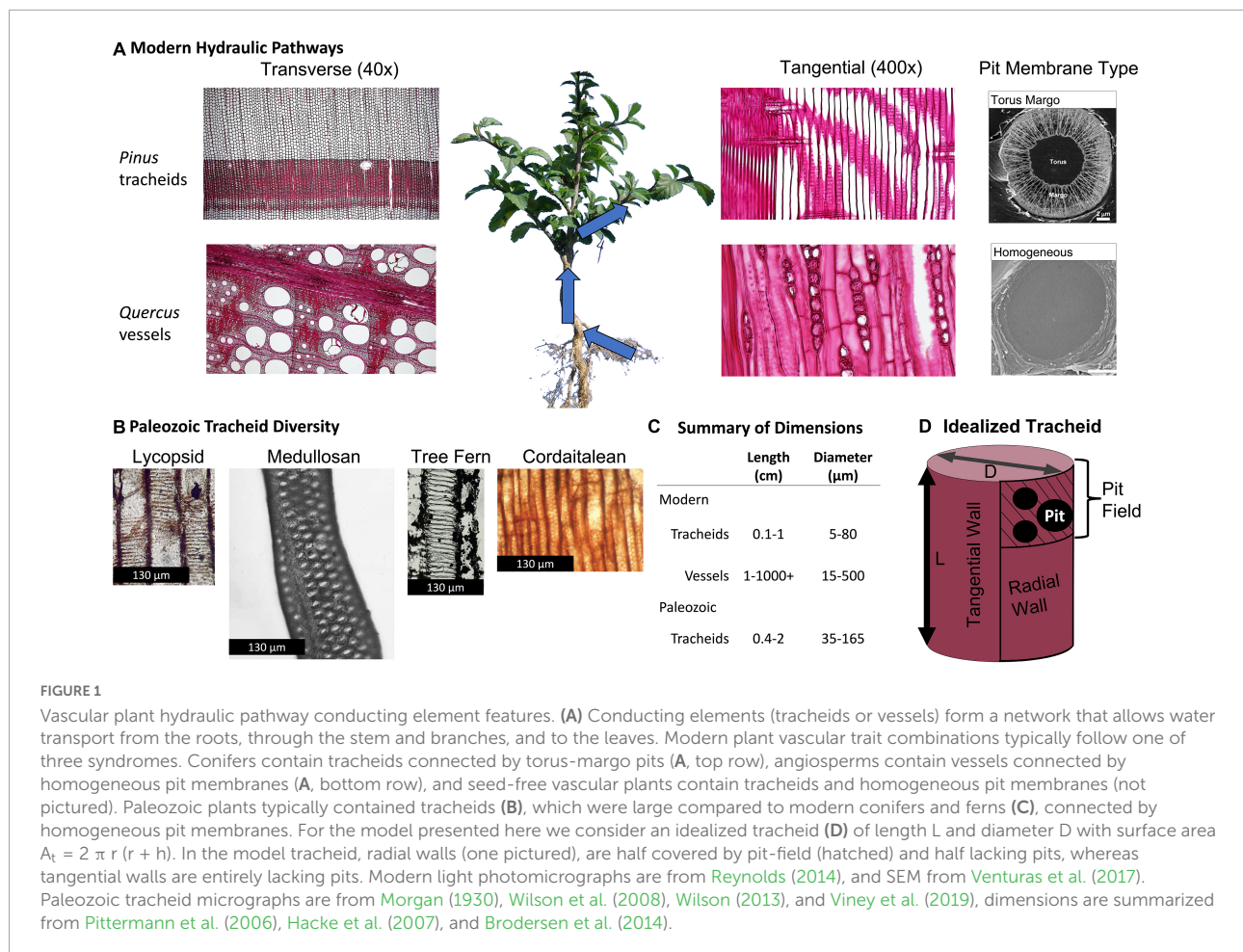
Morphological features of plant fossils are a well-established source of information about ancient Earth (McElwain, 1998; Royer, 2001; Beerling and Royer, 2002; Franks and Beerling, 2009; Peppe et al., 2011). For example, measurements of leaf fossil characteristics have been used to infer properties of ancient plant physiology (Boyce et al., 2009; Franks and Beerling, 2009; Brodribb and Feild, 2010; Nicotra et al., 2011; Haworth and Raschi, 2014; Haworth et al., 2014; Montañez et al., 2016; Wilson et al., 2017, 2020; Boyce and Zwieniecki, 2019; White et al., 2020) and greenhouse gas concentrations (Woodward, 1987; McElwain, 1998; Beerling and Royer, 2002; Wagner et al., 2002; Finsinger and Wagner-Cremer, 2009; Franks and Beerling, 2009; Steinthorsdottir et al., 2011; Montañez et al., 2016; Richey et al., 2020, 2021). Recently, these fossil derived properties have been incorporated into ecosystem process models (White et al., 2020; Matthaeus et al., 2021; Richey et al., 2021), and Earth system models (Macarewich, 2021) to assess terrestrial ecosystem carbon, water, and nitrogen cycles in deep time. Such models are critical for predicting Earth system changes, as they provide a unique opportunity to test hypotheses about Earth- and ecosystem processes by comparing their predictions about past changes to the geologic and fossil records.

Leaf physiology is of primary importance to models of vegetation. Leaf traits like stomatal conductance and mesophyll conductivity influence the rate of plant gas exchange of water vapor and CO_2 with the atmosphere. However, stomatal function is based on turgor pressure and therefore relies on water supply from xylem (McAdam and Brodribb, 2016; Cardoso et al., 2020; Holloway-Phillips, 2020). At the whole-plant scale, actively conductive tissue in woody stems and branches (i.e., sapwood) must be sufficient to supply the canopy with water (DeLucia et al., 1994; DeLucia et al., 2001; Meinzer et al., 2008; Zeppel and Eamus, 2008). Sapwood water transport is driven by the water potential (Ψ) gradient in xylem. However, xylem conductivity fails with excessively low water potential. That is, under dry and/or high evaporation conditions (decreasing negative Ψ), air is drawn into xylem (i.e.,

a cavitation event expanding into an embolism) which blocks water transport, causing loss of conductivity, gas exchange, and assimilation (Tyree and Sperry, 1989; Sperry et al., 1994; Hacke et al., 2006; Pittermann et al., 2013; Mayr et al., 2014). Cavitation-induced embolism is referred to as ‘failure’ as it inhibits the ability of xylem in sapwood to perform its primary role in providing water to the canopy, and causes plant death and limits plant distributions in modern ecosystems (Tyree and Sperry, 1989; Sperry and Tyree, 1990; Tyree and Ewers, 1991; Tyree and Zimmermann, 2002; Choat et al., 2012). The physiological limitations of xylem, therefore, represent a necessary link in the process-based representation of plants in ecosystem and Earth system models across natural history and today.

To demonstrate the importance of xylem limitation on ecosystem and plant function, and as a proof of concept for the feasibility of studying these processes across deep time, we present an updated version of the Paleo-BGC model from White et al. (2020) that simulates stem hydraulic limitations on leaf water supply based on a xylem structure-function relationship (presented in Section “Xylem physiology from fossils: Model background”). The previously published *Paleo-BGC* model is based on BIOME-BGC v4.1.2¹ (Thornton et al., 2002). Ecosystem process models simulate carbon, nitrogen, and water balances for vegetation and soil (Schimel et al., 2000; Thornton and Rosenbloom, 2005) as they are modified by a set of mechanistic representations of ecosystem processes (e.g., primary production, Farquhar et al., 1980; respiration, De Vries, 1975; Ryan, 1995; evaporation and transpiration, Penman, 1948; Monteith, 1965; Monteith and Unsworth, 2013). In BIOME-BGC these processes are driven by meteorology (e.g., temperature, photosynthetic active radiation, and precipitation) and modulated by sets of traits representing modern plant functional types (PFTs). White et al. (2020) developed *Paleo-BGC* to allow the representation of ancient ecosystems using relevant atmospheric properties and PFTs for extinct plants.

¹ <http://www.ntsug.umd.edu/project/biome-bgc.php>

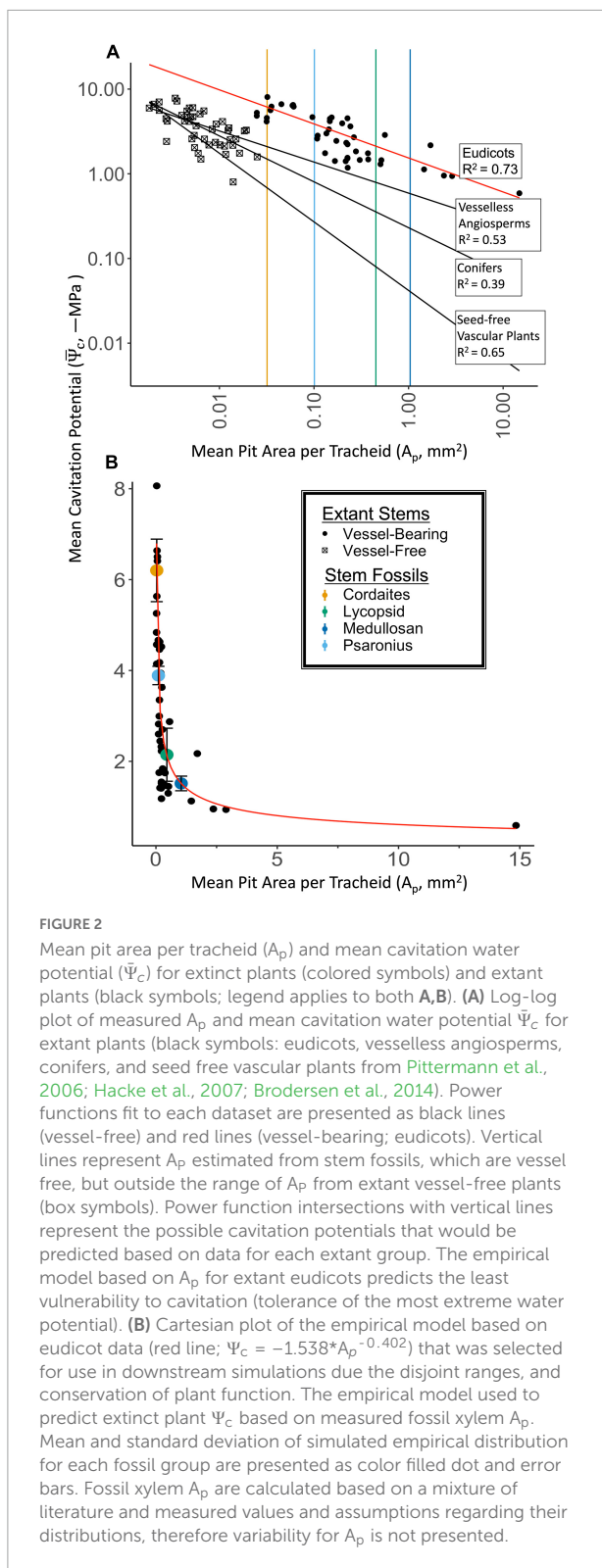


In particular, *Paleo-BGC* is modified to include extinct plant traits accessible through measurements made on fossil leaves and cuticle (see White et al., 2020 for further description). Here, we make a expand on *Paleo-BGCs* PFT trait repertoire and model logic in order to utilize a preliminary xylem morphological dataset from plant fossils that has been used in previous studies (Montañez et al., 2016; Wilson et al., 2017, 2020; Matthaeus et al., 2021), amended with novel data regarding an additional fossil parameter (pit-area per tracheid) that has an established structure-function relationship with xylem physiological limitation. Following work presented in these previous studies, we use paleoenvironmental parameters representing paleo-tropical plant types in the Pennsylvanian Subperiod of the Carboniferous Period plant to simulate ecosystem function using the updated *Paleo-BGC*.

The Carboniferous is a well characterized pre-angiosperm period with respect to paleo-flora and environmental conditions (e.g., see Falcon-Lang and Bashforth, 2004; DiMichele et al., 2006; Sahney et al., 2010; Bashforth et al., 2014; DiMichele, 2014; Montañez et al., 2016; Wilson et al., 2017, 2020), making it a generally auspicious target for paleoecological study. Here we focus on four Carboniferous paleo-tropical

dominant plant types: lycopsids, medullosans, tree ferns, and cordaitaleans. Lycopsids and medullosans are associated with ever-wet environments, whereas tree ferns and cordaitaleans are believed to have tolerated some aridity and/or moisture seasonality (DiMichele, 2014; Montañez et al., 2016; Wilson et al., 2017). Through the late Carboniferous and early Permian, progressive aridification beginning with the onset of moisture seasonality is implicated in repeated paleo-tropical vegetation restructuring events involving these four plant types (Dimichele et al., 2009; Montañez and Poulsen, 2013; Opluštil et al., 2013; Tabor et al., 2013). Further, xylem fossils from these groups show marked differences in anatomy, making the Carboniferous particularly interesting for the evaluating the role of xylem in extinct plant water transport, and the resulting differences between extinct and modern plants.

Generally, xylem comprised of less restrictive, larger water conducting elements is more susceptible to cavitation-induced embolism (presented in detail in section “Xylem physiology from fossils: Model background”). Based on this xylem structure-function relationship, the xylem of plants most associated with Carboniferous everwet tropical lowlands



(DiMichele, 2014; Wilson et al., 2017), notably lycopside (Cichan, 1985, 1986) and medullosans (Wilson et al., 2008, 2015; Wilson and Knoll, 2010; Wilson, 2013), are predicted to be

highly susceptible to cavitation-induced embolism. Plant types that became dominant in times and places experiencing aridity (i.e., cordaitaleans and tree ferns), on the other hand, may have been resistant to cavitation-induced embolism (Wilson et al., 2008; Wilson and Knoll, 2010; Wilson, 2013). To test these hypotheses using *Paleo-BGC*, we simulated these plants in a Pennsylvanian Subperiod tropical wetland location, with and without xylem limitation, to evaluate its effect on ecosystem processes. Pursuant to the comparison between extinct and extant plant function, we use the same conditions to simulate two extant plant taxa, which represent anatomical and ecological extremes using xylem anatomical data and cavitation water potential data from living plants (Hacke et al., 2006): *Morus alba* (common mulberry; Moraceae) and *Arctostaphylos patula* (greenleaf manzanita; Ericaceae).

Materials and methods

Xylem physiology from fossils: Model background

In leaves and stems, physiological limitation of xylem is related to its anatomy (Tyree and Sperry, 1989; Sperry et al., 1994; Hacke et al., 2006; Christman et al., 2012; Pittermann et al., 2013; Mayr et al., 2014) and can be estimated for extinct plants using measurements of fossils (Wilson et al., 2008, 2015; Wilson and Knoll, 2010; Wilson and Fischer, 2011; Wilson, 2013). In this study, we consider four major arborescent plant types from the Carboniferous Period: arborescent lycophytes (lycopside), medullosan pteridosperms (medullosans), stem-group marattialean tree ferns, and early-diverging coniferophytes (cordaitaleans) from the Carboniferous (see Wilson et al., 2017) for general description of plant types and natural history). Preserved xylem from these plant types has traditionally been used to inform phylogenetic differences.

The morphological properties of xylem fossil associated with these groups are different than most modern arborescent plants: nearly all plants in the Paleozoic Era contained xylem formed from a network of single-celled conduits closed at the ends, called tracheids. Tracheid cell walls contain porous zones spanned by homogeneous pit membranes through which water passed from one tracheid to another. In extant ecosystems, however, most arborescent plants have one of two combinations of xylem conduit type and pit membrane type (Figure 1). Most gymnosperm tree xylem conducts water through narrow (20–35 μm in diameter) single-celled tracheids with pit membranes that are differentiated into a non-porous zone (torus) and a porous zone (margo), forming a porous structure called torus-margo pits. Alternatively, most angiosperm trees contain wider xylem cells forming multicellular conduits, called vessels, which contain homogeneous pit membranes. There are a small

number of extant arborescent plants that share the same combination of features as Paleozoic plants: certain vesselless angiosperms and ferns have tracheids (i.e., they are ‘vessel-free’) with homogeneous pit membranes. Tracheids in vesselless angiosperms and ferns are relatively small, comparable in size to modern conifers (e.g., Pinales), and therefore can serve as functional analogs for the xylem anatomy of extinct coniferophytes, including the cordaitaleans (Pittermann et al., 2006, 2011; Hacke et al., 2007; Wilson et al., 2008; Figure 2). However, the tracheids found in fossil xylem associated with other key Carboniferous plant types (e.g., lycopsids and medullosans) are distinct from all of the aforementioned groups in their size (diameters in excess of 100 μm are common in some taxa, and length can exceed 20 mm) and pit membrane anatomy. Rather, they are more comparable with vessels in modern eudicot angiosperms (Cichan, 1985, 1986; Hacke et al., 2007; Wilson et al., 2008, 2015; Wilson and Knoll, 2010; Wilson, 2013, 2016; Table 1). This unusual combination of large, single-celled tracheids with homogenous pit membranes has been linked to an increased probability of sapwood dysfunction induced by xylem embolism (Cichan, 1986; Wilson et al., 2008, 2015, 2017; Wilson and Knoll, 2010; Wilson and Fischer, 2011; Wilson, 2013). Other well characterized differences between Paleozoic and modern xylem—such as the lack of secondary xylem in tree ferns, the prevalence of scalariform pits in tree ferns and lycopsids, and the fact that lycopsid secondary xylem is not the primary mechanical support for the stem (compiled in Taylor et al., 2009)—are not considered here, though the implications of some factors are discussed.

Although xylem cavitation and embolism are easily observed in plants, the mechanics of xylem hydraulic failure processes *in vivo* remain a topic of active study in plant physiology (see Venturas et al., 2017 for a review). Recently, pit membrane characteristics (i.e., pore constrictions and pit membrane thickness) have been implicated as a primary mechanism in the mechanics of xylem hydraulic failure (Thonglim et al., 2021; Avila et al., 2022; Levionnois et al., 2022), making them an obvious target for predictive modeling. However, pit membranes are rarely preserved in the fossil record. In this preliminary effort, we have therefore chosen to focus on more commonly preserved aspects of xylem anatomy and morphology. In particular, there is a robust relationship between the water potential at which air enters tracheids (i.e., “air-seeding pressure,” Ψ_C) and inter-tracheid pit area (A_p ; Wheeler et al., 2005; Hacke et al., 2006, 2007; Pittermann et al., 2006, 2011). That is, Ψ_C approaches zero with increasing A_p . In this modeling effort (described further in section “Model description” and **Supplementary material**), air seeding is assumed to be the primary cause of cavitation and embolism, as sufficient evidence exists from fossil to apply the structure-function relationship to extinct plants.

Xylem cells are well-preserved in the fossil record (Figure 1B), and pits can be observed and measured. The relationship A_p and Ψ_C can therefore be used to assess extinct plant taxa’s differential vulnerability to cavitation and subsequent loss of hydraulic conductance, or whether these plants are resistant to cavitation (Hacke et al., 2007; Figure 2). We have adapted this relationship for incorporation into the previously described ecosystem process model *Paleo-BGC* (Figure 3, White et al., 2020, and described further below).

At the whole-plant scale, the ability of sapwood to supply water for transpiration, and photosynthesis depends on the allometric relationship between sapwood and canopy (DeLucia et al., 1994; Delucia et al., 2001; Meinzer et al., 2008; Zeppel and Eamus, 2008). Reduction of maximum sapwood conductivity occurs when sapwood transitions to heartwood (sapwood turnover; Chattaway, 1952), and recovery of maximum conductivity occurs when new sapwood grows (Venturas et al., 2017). Therefore, we connect the ratio of sapwood to canopy carbon simulated by *Paleo-BGC* ($C_{SW}:C_L$) to the capacity of the sapwood to supply the canopy with water. This is similar to Leaf Specific Conductivity (Ewers, 1985), but is expressed here in terms of biomass ($C_{SW}:C_L$), which utilizes modeled carbon pools that currently exist in *Paleo-BGC* and does not require information about sapwood area (see section “Materials and methods”).

Model description

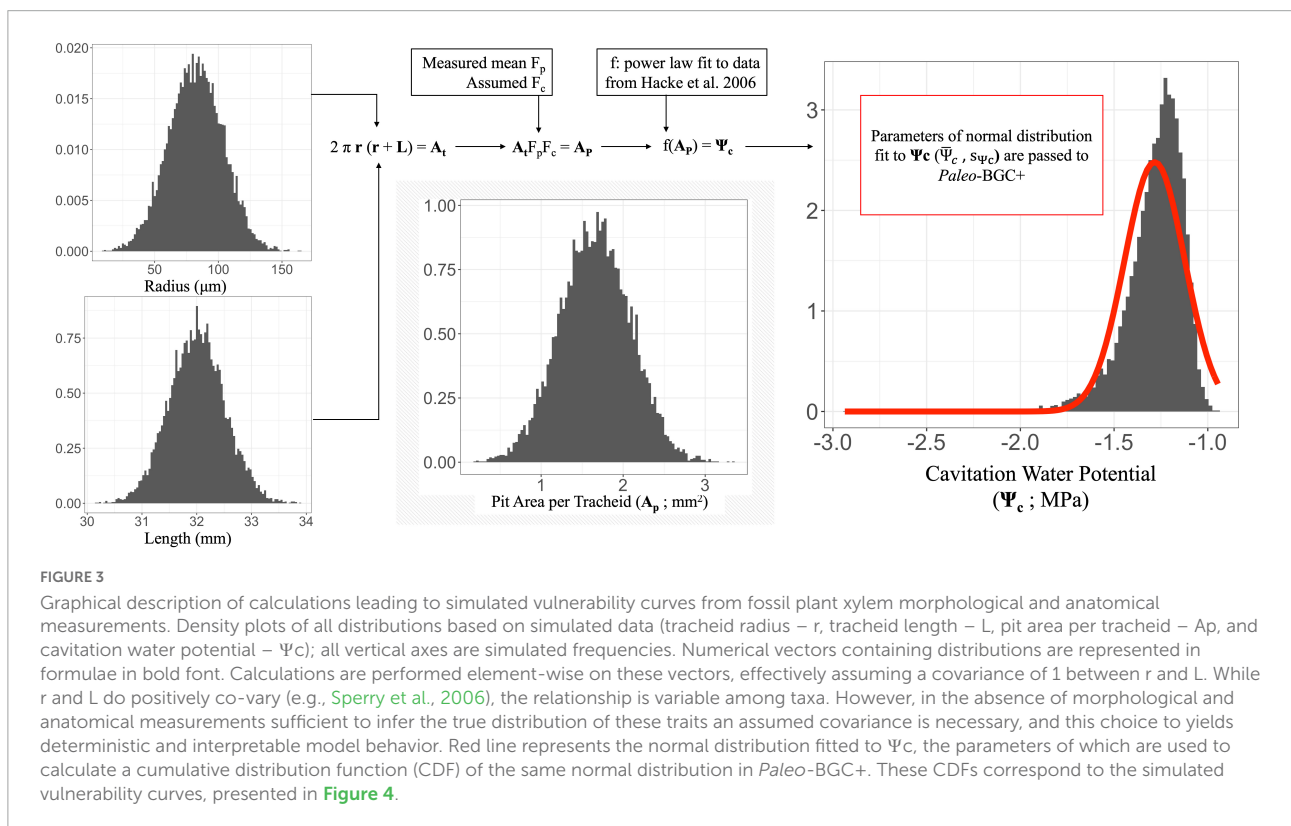
In the published version of *Paleo-BGC* (White et al., 2020), models of extinct plants are represented by two sources of parameters, primarily measurements of leaf fossil material, and by leaf functional traits. These traits include mesophyll conductance, hydraulic conductivity, nutrient ratio (C:N), Specific Leaf Area, boundary layer conductance and maximum stomatal conductance, in the context of ecosystem processes. Here, we add model components that further limit water supply to leaves due to sapwood dysfunction. This updated model version, referred to here as *Paleo-BGC+*, represents xylem loss of conductivity and restricted recovery based on xylem anatomy and sapwood-canopy allometry utilizing plant fossil information as input.

To model the embolism component of sapwood dysfunction, we assume that the failure of xylem and loss of conductivity (i.e., cavitation-induced embolism) is primarily the result of air-seeding. In the current model update, loss of conductance proceeds with decreasing water potential as tracheids embolize sequentially along a gradient of morphological traits that are assumed to be normally distributed in the xylem tissue. Based on these assumptions, and following the rationale of Hacke et al. (2006), we consider the mean cavitation water potential ($\bar{\Psi}_C$) to be that which induces cavitation and loss of conductivity in the average tracheid.

TABLE 1 Morphophysiological characteristics of fossil xylem from extinct plants and comparison with extant taxa.

Group	F_p (dim)	L(mm)	D(μ m)	A_t (mm^2)	A_p (mm^2)	$\bar{\Psi}_c$ (-MPa)
Lycopsid	0.08	17*	110*	5.9	0.45	2.2
Medullosan	0.10	20†	165†	10.4	1.04	1.5
Tree Fern	0.07	6‡	75§	1.4	0.10	3.89
Cordaitalean	0.07	4†	35†	0.4	0.03	6.2
EBF-V	0.05	162	57	29.0	1.46	1.13
EBF-R	0.04	32	25	2.5	0.10	4.67

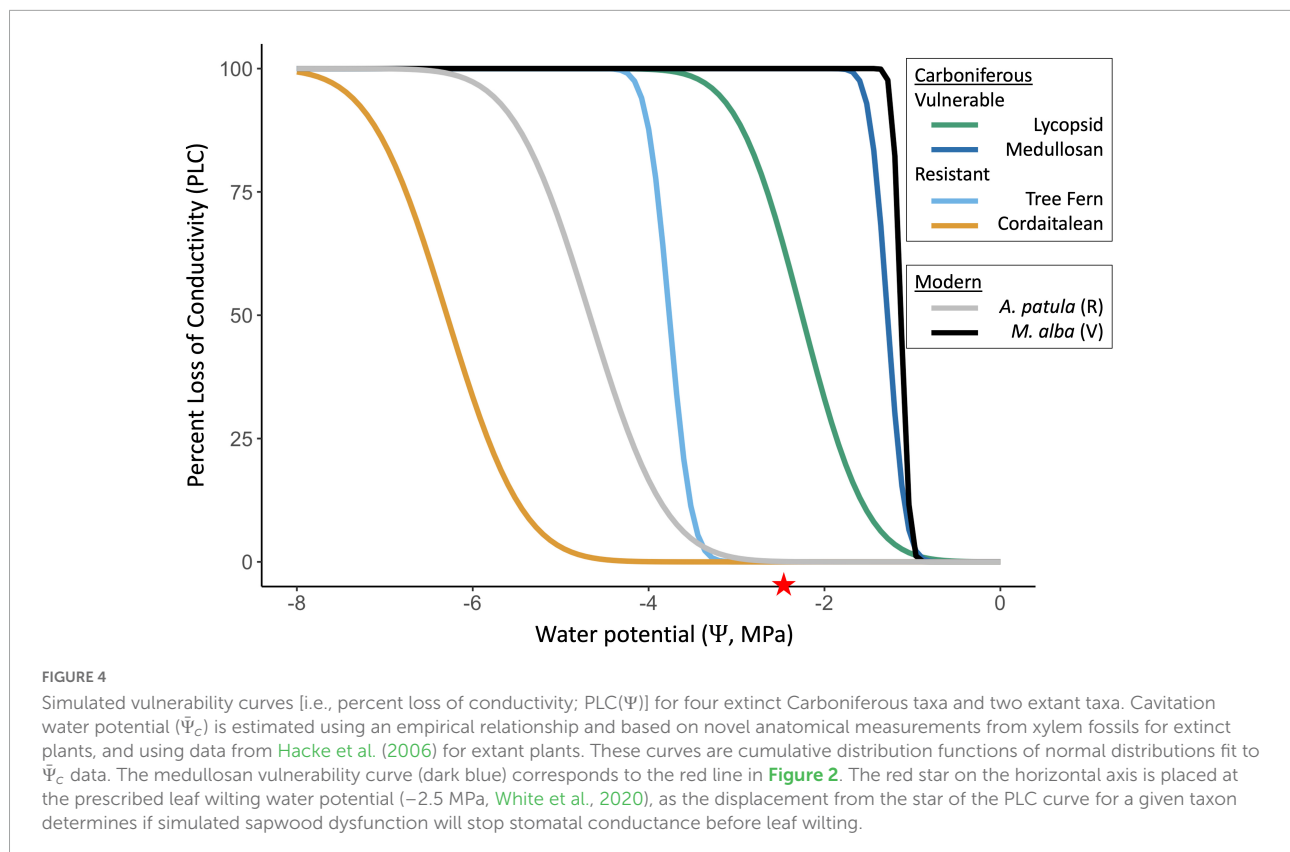
Extinct plant xylem cells are all tracheids, whereas extant taxa are vessel-bearing. Pit fraction (F_p , dimensionless, the areal fraction of tracheid pit-field segments occupied by pits), tracheid length (L), and diameter (D) were used to calculate tracheid surface area (A_t), pit area per tracheid (A_p), mean embolism water potential ($\bar{\Psi}_c$, i.e., the water potential inducing cavitation and loss of conductivity in the average tracheid). Representative literature values for Carboniferous xylem fossils originate as follows: Lycopsids from Cichan (1985) (*), Medullosans and Cordaitaleans from Wilson (2013) (†), Tree Fern from Morgan (1930) (§), and White (1962) (average of 3 marattialean NLR, ‡). Shading indicates values for extant taxa represented by evergreen broadleaf forest (EBF) parameters provided with *Paleo*-BGC in combination with properties of *Morus alba* (EBF-V), and *Arctostaphylos patula* (EBF-R) from Hacke et al. (2006); parameters from *Morus* and *Arctostaphylos* refer to values from vessels, not tracheids. Calculated values are in italics.



Therefore, we model percent loss of xylem conductivity with decreasing water potential [PLC(Ψ), i.e., the “vulnerability curve,” Figures 3, 4] as a normally distributed random variable with mean $\bar{\Psi}_c$ and standard deviation s_{Ψ_c} . The cumulative distribution function of PLC(Ψ) replicates the general shape of many vulnerability curves observed in living plants (Tyree and Sperry, 1989; Hacke et al., 2007; Christman et al., 2012; Jinagool, 2015), and can be used to represent a variety of underlying causes of xylem failure.

It has been shown that there is wide variation in xylem cell morphology and distribution that corresponds to an equally wide variation in the shape of PLC curves, reflecting plant

adaptation to a range of environmental parameters (e.g., Pittermann et al., 2013; Rico et al., 2013). Therefore, the normal distribution is used here as a preliminary modeling convention in the absence of more thorough data stem xylem. Other distribution shapes may better represent the shape of PLC curves in some taxa, for which PLC is determined primarily by factors other than air-seeding or the underlying morphological distributions are non-normal (e.g., tracheid implosion, or multimodal tracheid/vessel size distributions as may be the case for tree fern water transport through meta- and proto-xylem; Zimmermann et al., 1982; Carlquist, 2009; Domec et al., 2009). Nonetheless, the focal Carboniferous taxa



described here lack vessels, and air seeding generally occurs at higher water potentials than tracheid implosion (Domec et al., 2009, but see Discussion below). Further, there is presently no database of fossil xylem measurements sufficient to reliably infer the true distribution of the relevant parameters (i.e., see Table 1 and below), particularly in the case of pit area per tracheid (A_p). Finally, the normal distribution can be efficiently implemented using its moments (i.e., mean and standard deviation, Figures 2, 3). As an initial test of the potential importance of sapwood to ecosystem processes, therefore, we chose to use the normally distributed PLC curve to analytically connect PLC to measured xylem morphology (Figures 2–4).

The additive inverse of PLC is proportional to a new scalar [i.e., remaining sapwood conductivity; $1 - (\text{PLC}/100) = m_{sw}$] that is multiplied into the existing series of environmental scalars (e.g., vapor pressure deficit, freezing soil temperatures) in Paleo-BGC. These scalars reduce stomatal conductance from the maximum values derived from plant fossils for each plant type (Jarvis and Mcnaughton, 1986; White et al., 2020). In this new version, operational stomatal conductance now also depends on the capacity of bulk sapwood to supply water to the canopy (see below), which itself is a function of xylem morphology and PLC.

To predict PLC, we first consider pit area per tracheid (A_p) as a primary morphological predictor of mean cavitation water potential. Pit area itself depends on tracheid surface area (A_t) and the fraction of surface area that is occupied by inter-tracheid

pits (Wheeler et al., 2005; Hacke et al., 2006, 2007; Pittermann et al., 2006, 2011). We estimate the distribution of A_p for fossil taxa based on several tracheid morphological traits that are measurable in fossil xylem including: tracheid length (L), diameter (D), and the fraction of inter-tracheid surface occupied by pits (F_p) referred to as the pit-field fraction (Hacke et al., 2006; see Figure 1D).

We obtained tracheid morphological properties for each plant group through a mixture of sample measurements, and reported literature values. A summary of values and their sources are provided in Table 1. We used these values in calculations based on simplifying assumptions as follows: to approximate distributions of tracheid surface area (A_t) we used published values of L and D from Morgan (1930), White (1962), Cichan (1985) and Wilson (2013) for Carboniferous plant groups. From these data, we assumed that the midpoint of the ranges presented for L and D are the mean, and that the extreme values are each two standard deviations from the mean. Using these literature derived means and standard deviations, we simulated normally distributed empirical data for L and D using the R command *rnorm* with $n = 10,000$ (R Core Team, 2021). These distributions form the basis for the within-taxon variation in A_p and the dispersion of PLC(Ψ) (described below and see Figures 2–4).

To compare the fossil plant types to extant plant functioning, we also used the same xylem morphological

properties to simulate A_p distributions for two extant taxa reported in Hacke et al. (2006): white mulberry (*Morus alba*, referred to as V for ‘vulnerable’) and greenleaf manzanita (*Arctostaphylos patula*, referred to as R for ‘resistant’). Parameters prescribing predicted PLC curves (i.e., $\bar{\Psi}_c$ and s_{Ψ_c}) for each extant taxa are characterized were combined with an existing *Paleo*-BGC plant functional type (PFT) for evergreen broadleaf forest (EBF), to produce an amended PFT representing modern plant types that are vulnerable (EBF-V) and resistant (EBF-R) to sapwood dysfunction.

Differing tracheid morphology among taxa, specifically tracheid geometry and pit anatomy, makes direct quantitative comparison based on morphological properties challenging, particularly in the absence of comprehensive descriptions of tracheid morphological variation in the xylem of each fossil taxon. To facilitate quantitative evaluation of the effect of morphological traits, we model hydraulic properties of an idealized tracheid using the morphological properties of each taxon (see Figure 1D, schematic of idealized tracheid). All tracheids are modeled as having a circular cross section and flat ends (i.e., a right circular cylinder of length L and diameter D , Figure 1). In fossil taxa, we assume that half of each radial wall is in hydraulic contact with adjacent tracheids and pit-bearing (i.e., the contact fraction, F_c , Hacke et al., 2006; Wilson et al., 2008; Wilson and Fischer, 2011), and that tangential walls are without pits. Therefore, the contact fraction is set to 25% for all fossil taxa.

We measured the pit-field fraction for Carboniferous plant groups from scanning electron micrographs (SEM) and light micrographs of tracheid walls in fossil xylem macerations. The area of each well-preserved, continuous segment of pit-bearing tracheid wall (i.e., a fragment of the pit-field; $A_s = L_s * W_s$; see Figure 1D) was measured, along with the length (l) and width (w) of each pit in that segment. The area of each pit was approximated as an ellipse ($A = \pi l w$). Pit areas in each segment were summed and divided by that segment’s area to calculate the pit fraction per segment ($F_{p,s} = \Sigma A/A_s$). We assume that the average pit fraction per segment ($F_{p,s}$) is equal to the pit-field fraction for each fossil taxon, that is, that the pits are distributed uniformly within the pit-field. Then, the pit fraction (F_p) of the tracheid is calculated as the product of pit-field fraction ($F_{p,s}$) and contact fraction for tracheid fossils. Tracheid length (L) and diameter ($D = 2r$) were then used to calculate a distribution of idealized tracheid surface area [$A_t = 2 \pi r (r + L)$]. We assume perfect covariance between the simulated empirical distributions of L and D within plant type, therefore the A_t calculation was applied to L and D distributions element-wise (see Figure 1D). Pit area per tracheid ($A_p = F_p F_c A_t$) was then calculated for each value of the mean of F_p for each plant type and assumed F_c of 0.25. Variation in L and D , therefore, is source of dispersion in A_p and PLC (see Supplementary material).

To estimate the water potential at which cavitation would occur, we fit a power law (f) relating simulated empirical data for A_p to the mean cavitation pressure (i.e., the mean water potential of the distribution of conductivity as a function of water potential, $\bar{\Psi}_c$) from Hacke et al. (2006) for eudicots (red line in Figure 2 and Table 1). We used this power law to calculate cavitation water potential [$\Psi_c = f(A_p)$] across the simulated distribution of A_p for each taxon (Figure 3).

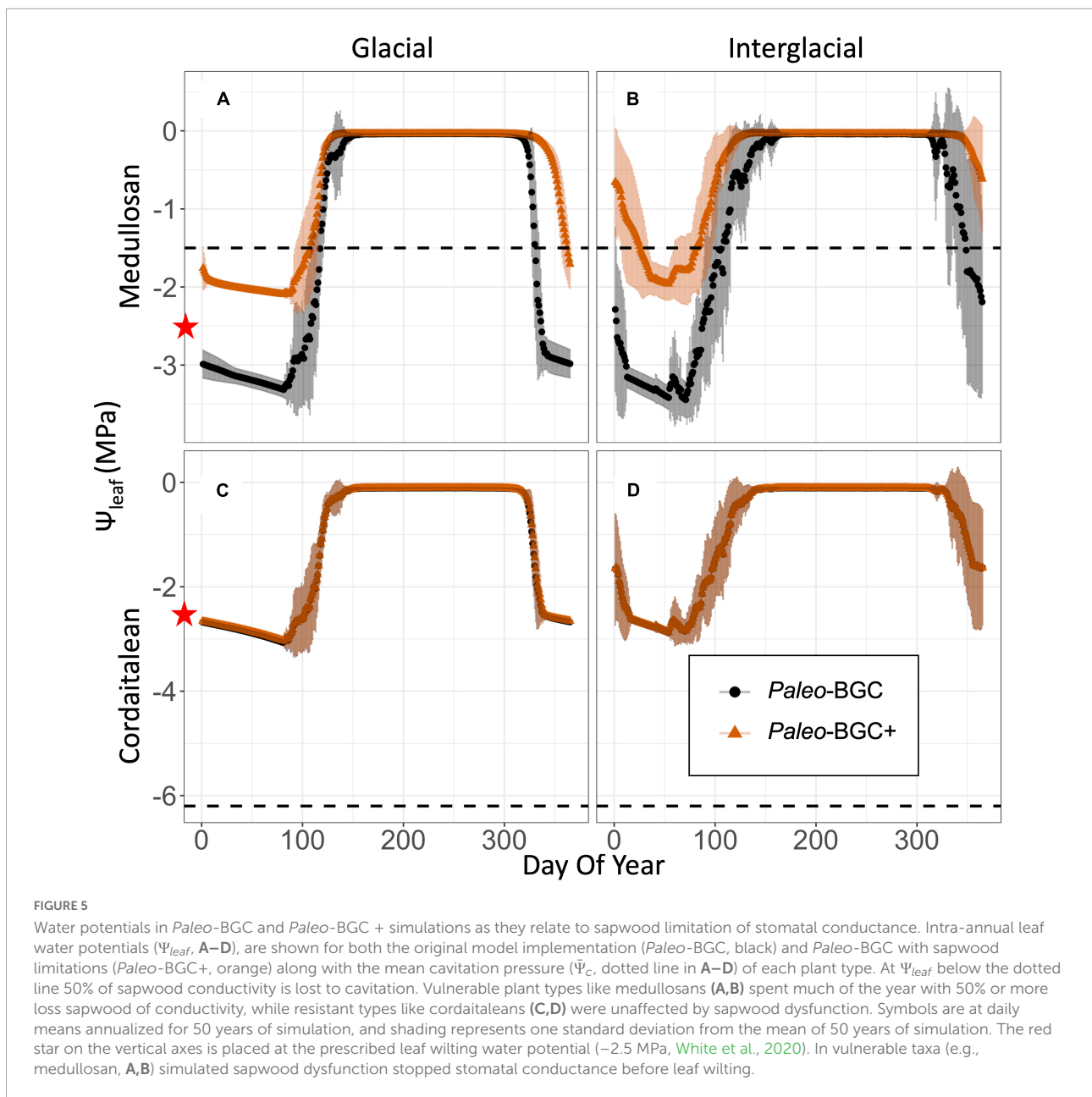
To facilitate PLC inclusion in the new implementation of *Paleo*-BGC, we then fit a normal distribution to the simulated Ψ_c distribution for each plant type [$\mathcal{N}(\bar{\Psi}_c, s_{\Psi_c})$, Figures 3, 4 and see section “Discussion”). We then estimate PLC at any given water potential (Ψ) using the moments $\bar{\Psi}_c$ and s_{Ψ_c} for each plant type to calculate the cumulative probability of \mathcal{N} :

$$PLC(\Psi) = 0.5 * \operatorname{erfc} \left(\frac{\bar{\Psi}_c - \Psi}{s_{\Psi_c} \sqrt{2}} \right) \quad (1)$$

where erfc is the complementary error function. During simulation in *Paleo*-BGC, when conditions are becoming drier, changes in leaf water potential (Ψ_{leaf}) are used to calculate $PLC(\Psi_{leaf})$. We use Ψ_{leaf} to drive PLC to estimate near-leaf sapwood dysfunction as a result of air-seeding embolism, as near-leaf xylem likely experiences the most extreme water potentials (Koçillari et al., 2021). The additive inverse of $PLC(\Psi_{leaf})$, corresponding to the remaining sapwood conductivity [$1 - PLC(\Psi_{leaf}) = m_{sw}$] is multiplied into the existing scalar reduction stomatal conductance (g_s) as a result of xylem cavitation-induced embolism (Figure 4). Under re-wetting conditions PLC and g_s are held at local minima pending prescribed primarily xylem regrowth, and secondarily, bubble dissolution (see Supplementary material and Supplementary Figure 3), introducing hysteresis to the calculation of g_s in *Paleo*-BGC.

During the wet season, we assumed embolism recovery to be dominated by sapwood regrowth (Utsumi et al., 2003; Venturas et al., 2017). The wet season was prescribed to begin after modeled soil moisture, and therefore leaf water potential had reached annual plateaus (Figures 5, 6 and Supplementary Figures 1, 3, and refer to White et al., 2020), during which we set conductivity to recover at a rate of 1% per day to simulate the growth of new sapwood.

To capture the limitation imposed by embolized xylem in bulk sapwood on water supply to the canopy—the second avenue of sapwood dysfunction modeled here—we utilized the sapwood turnover and carbon allocation variables. In. to *Paleo*-BGC (White et al., 2020), its predecessor BIOME-BGC, sapwood turnover occurs at a rate that is proportional to annual maximum sapwood and a prescribed constant ($t_{sw} = 0.7$) set by the user. In the initial descriptions of the parameterizations for BIOME-BGC described in White et al. (2000), it is noted that there was insufficient data to inform t_{sw} . We therefore propose that sapwood containing embolized xylem is available for turnover and have set t_{sw} to vary in linearly with PLC,



while maintaining a minimum annual sapwood turnover of 25% (see section “Discussion”). We consider this a null model with respect to responses to xylem embolism as it does not constitute an active response, but rather is a necessary consequence of loss of sapwood function. We then assumed that the originally prescribed allocation of carbon to new sapwood relative to new canopy ($C_{new,SW}:C_{new,L}$) represents the ideal ratio to supply the canopy foliage with water. Unlike sapwood turnover, this allometry is well supported ([White et al., 2000](#)).

Based on these assumptions we calculate a sapwood-canopy allometric cap for theoretical stomatal conductance. Following [White et al. \(2020\)](#), we use the ecophysiological constants for evergreen broadleaf forest (EBF: $C_{new,SW}:C_{new,L} = 0.22$) as they

are most comparable to the focal Paleozoic taxa. We assume that this ratio provides sapwood conductivity that is exactly sufficient to achieve maximum stomatal conductance ($g_{s,max}$). Actualized $C_{SW}:C_L$ are calculated daily by *Paleo-BGC*, and vary freely from this ratio based on assimilation, nitrogen limitation, and sapwood C remaining after turnover. When $C_{SW}:C_L$ is reduced below the sufficient ratio, we reduce maximum stomatal conductance ($g_{s,max}$) in proportion. This represents sapwood water transport dysfunction as a result of the allometric deficit of sapwood relative to canopy:

$$g_{s,max}^* = g_{s,max} * \frac{C_{SW} : C_L}{C_{new,SW} : C_{new,L}} = g_{s,max} * R_{max}^* \quad (2)$$

TABLE 2 Fossil informed stomatal conductance parameters.

Group	$g_{s,max}$ (m/s)	$g^*_{s,max}$ (m/s)
Lycopsid	3.3	1.9
Medullosan	1.4	0.8
Tree Fern	0.3	0.3
Cordaitalean	0.4	0.4
EBF-V	0.2	0.1
EBF-R	0.2	0.2

Maximum stomatal conductance ($g_{s,max}$), estimated from fossil leaf traits (Montañez et al., 2016; White et al., 2020; Wilson et al., 2020), is taken from base *Paleo-BGC* input files for each group. New to *Paleo-BGC+*, maximum stomatal conductance is dynamically scaled for sapwood allometric deficit ($g^*_{s,max}$). Maximum value of $g^*_{s,max}$ in the final simulation year is presented to facilitate direct comparison to fossil leaf informed $g_{s,max}$. Plant types that experienced sapwood deficit with reduced maximum stomatal conductance are bolded. Shading indicates values for extant taxa represented by evergreen broadleaf forest (EBF) parameters provided with *Paleo-BGC* in combination with properties of *Morus alba* (EBF-V), and *Arctostaphylos patula* (EBF-R) from Hacke et al. (2006); parameters from *Morus* and *Arctostaphylos* refer to values from vessels, not tracheids.

where $g^*_{s,max}$ is the maximum stomatal conductance allowed by the available sapwood, and R^*_{max} is the current biomass sapwood:canopy allometry as proportion of the assumed sufficient allometry. This allometric cap on stomatal conductance, is applied only when there is a sapwood deficit ($R^*_{max} < 1$), and operational stomatal conductance ($g_{s,op}$) is greater than $g^*_{s,max}$. Under these conditions $g_{s,op}$ is set to $g^*_{s,max}$, otherwise calculation of stomatal conductance is unaltered. Representative values of $g^*_{s,max}$ are presented in Table 2 alongside $g_{s,max}$. We provisionally refer to the model implementation that includes physiological limitation due to sapwood dysfunction as *Paleo-BGC+* when distinguishing between the two implementations. As the two modes of simulated sapwood dysfunction are non-independent (i.e., embolism drives sapwood allometric deficit), they are referred to collectively as sapwood dysfunction in most cases. Representative annual values for the modifications introduced here are presented in Figure 6, but are heavily dependent on meteorology (described below). Model code for *Paleo-BGC+* is available at github.com/wjmatthaeus/.

Meteorological setting and experimental design

In addition to the ecophysiological inputs describing the vegetation, *Paleo-BGC* is driven by meteorological inputs (e.g., daily data from a climate model). To evaluate the effect of stem limitation on ecological functioning in the Pennsylvanian Subperiod, two sets of ecosystem process simulations were driven by the meteorological inputs representing the same location as (White et al., 2020). Global climate simulations from GENESIS v3 (Thompson and Pollard, 1997; Alder et al., 2011) were used to generate meteorological inputs representing

a single tropical wetland location from what is now the Illinois Basin. Parameterization of GENESIS v3 for the Late Paleozoic consisted of Sakmarian (~290 Ma) continental configuration and topography (after the description of Ziegler, Hulver, and Rowley in Martini, 1997), 2.5% reduction in solar luminosity (Gough, 1981), a circular orbit with 23.5° obliquity (Horton et al., 2010). To represent extremes of Pennsylvanian climate, and to allow comparison to Matthaeus et al. (2021) we used peak glacial and interglacial atmospheric compositions of 182 ppm CO₂, and 546 ppm CO₂, respectively, and 28% O₂.

From each of these GENESIS v3 parameterizations, 10 years of daily temperature (minimum, maximum and average, °C), precipitation (cm day⁻¹) and solar radiation (W m⁻²) were taken directly. Additionally GENESIS v3 derived daily minimum/maximum temperature, precipitation, and paleolatitude were used to calculate vapor pressure deficit (VPD, Pa) and day length (s) with the MT-CLIM model (Running and Coughlan, 1988²). These simulated meteorological scenarios (Table 3 and Supplementary Figure 1) were classified as tropical and subhumid by White et al. (2020) with a wet season from early spring to early winter, and at least 2 months without precipitation during the summer on average. Each meteorological scenario was used to parameterize *Paleo-BGC* simulations using each plant type.

To isolate the effect of xylem physiological limitation on simulated ecosystem water cycling and productivity for both modern and Carboniferous plant types, we performed the following experiment. As described in Section “Xylem physiology from fossils: Model background” and Supplementary material, each plant type was assigned a set of xylem vulnerability and refilling parameters. For each combination of plant type and meteorological scenario we simulated 50 years of ecosystem processes using two models: (1) using the unaltered, original model (*Paleo-BGC*) and (2) using the model with sapwood dysfunction added (*Paleo-BGC+*).

Results

Pit fraction (F_p) varied among the fossil plant types measured. Medullosan tracheid fragments had the highest pit fraction ($F_p = 0.1$, Table 1), followed by lycopsid tracheids ($F_p = 0.08$). Tree fern and cordaitaleans tracheid fragments had the lowest pit fraction among fossil plant types ($F_p = 0.07$). Extant plant types—the vulnerable mulberry (EBF-V) and the resistant manzanita (EBF-R)—had lower pit fraction than fossil plant types. Differences in tracheid length (L) and diameter (D) contributed more to differences in pit area per tracheid (A_p) than pit fraction: wider and longer tracheids had more pit area per tracheid than

² <https://www.nts.gov/umt.edu/project/mt-clim.php>

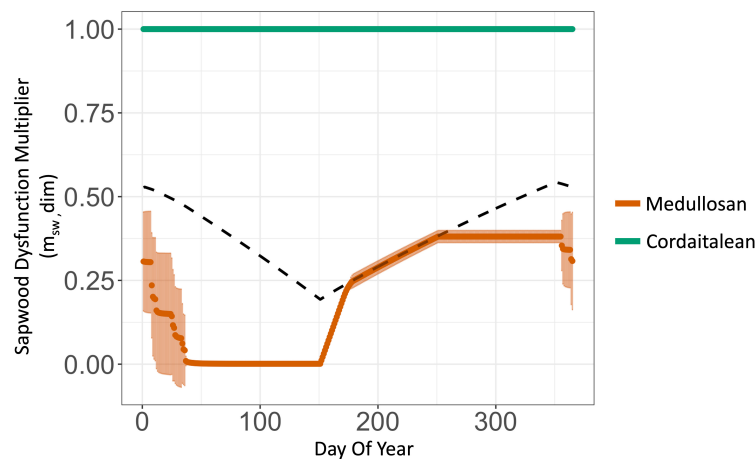


FIGURE 6

Multiplier representing the proportional reduction in stomatal conductance as a result of by sapwood dysfunction due to embolism ($m_{sw} = 1 - PLC/100$) and insufficient sapwood allocation (R_{max}^* , dotted line). Stomatal conductance is unaffected in plant types resistant to sapwood dysfunction (cordaitalean, green), and reduced in vulnerable plant types (e.g., medullosan, orange). Medullosans were impacted by sapwood dysfunction because of their wide tracheids ($165 \mu m$) and high pit area per tracheid ($1.04 mm^2$). The increase in m_{sw} beginning at day 150 represents xylem regrowth at the start of the wet season. The dotted line represents the upper bound placed on stomatal conductance of the medullosan due to a sapwood:canopy allometric deficit (R_{max}^*) as a result of sapwood loss due to cavitation. For the cordaitalean R_{max}^* was greater than one and therefore is not pictured. Only the final simulation year is presented.

narrow tracheids with high pit fractions. Medullosans had the highest pit area per tracheid ($A_p = 1.04 mm^2$) and highest mean cavitation pressure ($\bar{\Psi}_c = 1.5$), making it the most vulnerable to sapwood dysfunction among these fossil plant types. Lycopside are the next most vulnerable (Table 1). Therefore, lycopsids and medullosans are referred to as 'vulnerable plant types.' Finally, tree ferns and cordaitaleans, which have the lowest cavitation water potentials (Table 1), are referred to as sapwood dysfunction 'resistant plant types.'

The two new models of sapwood dysfunction implemented in *Paleo-BGC+*—the proportional reduction in operational stomatal conductance due to embolism (m_{sw} , Figure 6) and sapwood allometric insufficiency limiting maximum stomatal conductance ($g_{s,max}^*$, Table 2 and Figure 6)—interacted to reduce stomatal conductance compared to the previously published model version (Figure 7, black vs. orange boxes). This effect was observed in vulnerable plant types (i.e., high A_p and $\bar{\Psi}_c$, lycopsid and medullosan), but not resistant plant types (tree ferns and cordaitaleans). Embolism began in the dry winter season, when low precipitation (Table 3 and Supplementary Figure 1) drove low leaf water potentials relative to the stem hydraulic limitations of vulnerable plant types (i.e., $\bar{\Psi}_c$, dotted lines in Figures 5A–D and Supplementary Figure 2), which coincided with a proportional reduction in operational stomatal conductance for vulnerable plant types (m_{sw} , orange lines in Figure 6), but not for resistant plant types (green line, Figure 6). Simulated embolism also resulted in accelerated sapwood turnover and proportionally reduced sapwood-canopy biomass allometry (R_{max}^* , Figure 6, dotted line) and reduced

TABLE 3 Summary of the meteorological input scenarios to *Paleo-BGC* and *Paleo-BGC+*.

Scenario	T_{ave} (°C)	Precipitation (cm)	No. of days with precipitation
Glacial: 182 ppm CO ₂ 28% O ₂	23	0.4	246
Interglacial: 546 ppm CO ₂ 28% O ₂	28	0.5	301
Interglacial: 600 ppm CO ₂ 28% O ₂	29	0.5	296

Simulation averages are presented. Days with precipitation occurred seasonally.

maximum stomatal conductance ($g_{s,max}^*$, Table 2), particularly during simulated xylem regrowth at the start of the wet season.

Reduced stomatal conductance due to sapwood dysfunction slowed simulated water use in *Paleo-BGC+* as compared to *Paleo-BGC*, which does not simulate sapwood dysfunction (Figures 7A,B). Vulnerable plant types therefore left more water in the soil, increasing average stream flow (Figures 7C,D). Resistant plant types were unaffected by the addition of sapwood dysfunction to the model, and showed no change in stomatal conductance, water use, soil water or stream flow. As *Paleo-BGC* and related models are limited to single plant-type simulations (e.g., as in monotypic stands), slowed water use in *Paleo-BGC+*, also extended the growing season (days with $\Psi_{leaf} > -2.5 MPa$) by up to 19 weeks in vulnerable plant groups (Figure 5 and Supplementary Figure 3). Slowed water use was more

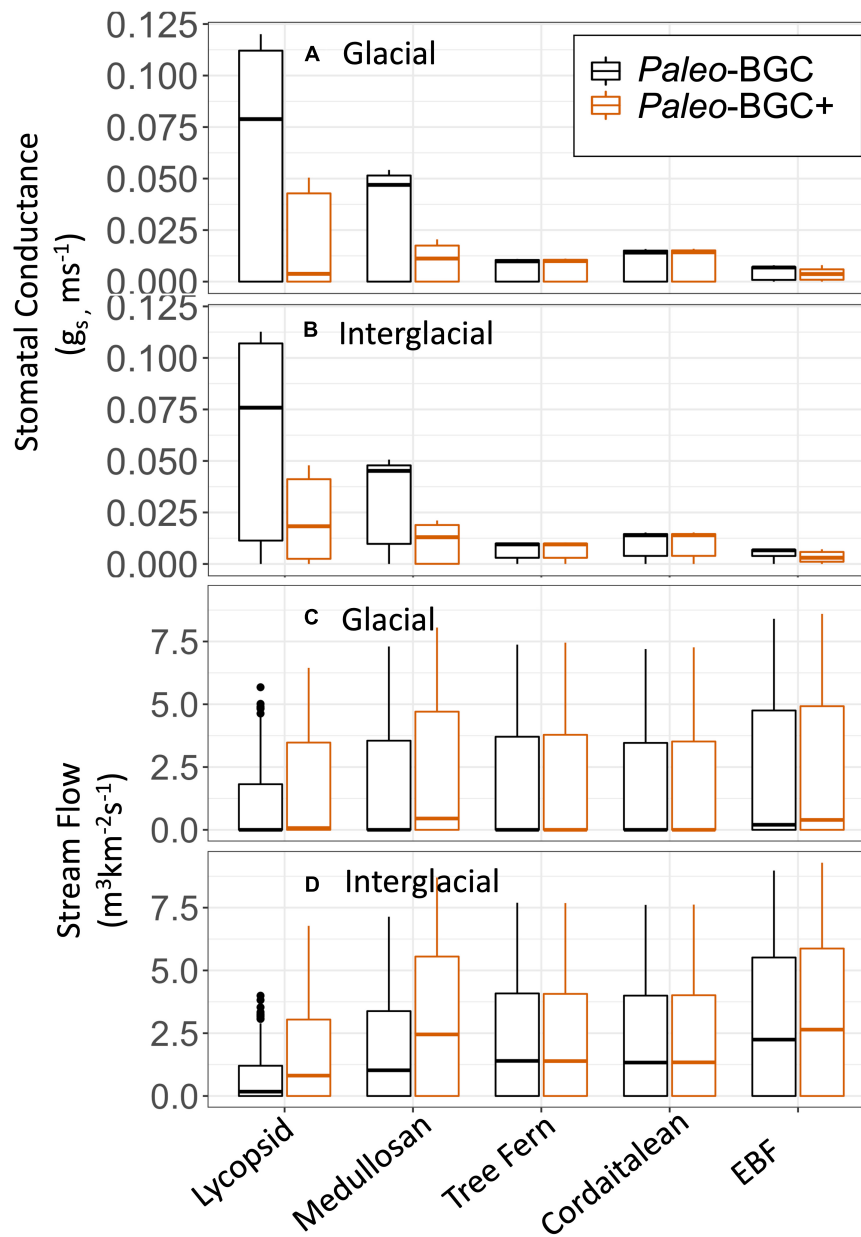


FIGURE 7

Simulated average water cycle fluxes from two ecosystem process model implementations (*Paleo-BGC*, *Paleo-BGC+*) that differ in their representation of sapwood physiological limitation of stomatal conductance. Four fossil and two extant plant types were simulated under tropical wetland conditions in the Carboniferous Period. Stomatal conductance (g_s , A,B) was reduced and stream flow increased (C,D) for plant types that are vulnerable to sapwood dysfunction (lycopsid and medullosan). Extant plant types (EBF-V, EBF-R) are averaged to clarify presentation (EBF).

pronounced in the Glacial Scenario (Figures 7A,C), whereas the change in runoff was greater in the Interglacial Scenario (Figures 7B,D). This slowing of the water cycle was most prominent in taxa with high $g_{s,max}$, the lycopsid and medullosan types. With sapwood dysfunction considered, lycopsids were no longer the fastest water users in the glacial scenario, as they are using the original *Paleo-BGC* model. Rather, lycopsids used water slowest of all simulated plant types in the glacial scenario.

Simulated biomass was also impacted by the inclusion of sapwood dysfunction in *Paleo-BGC+*. For vulnerable plant types, mean leaf area index (LAI, m^2 canopy m^{-2} ground) and vegetation biomass (leaf, stem, and root C) were reduced as compared to results from *Paleo-BGC* (Table 4, red cells), particularly in the Glacial scenario. Resistant plant types showed little or no change in LAI and vegetation biomass (un-colored cells, <10% change). The largest reductions in biomass occurred

in the vulnerable medullosans, which lost 50–60% of its biomass in both Glacial and Interglacial scenarios. The notable exception to the trend of reduced biomass in *Paleo-BGC+* is the stem and root carbon accumulation of the cordaitaleans in the Glacial scenario (green cells). Whereas the addition of dynamic sapwood turnover rates limited medullosan productivity and sapwood mass, it allowed the resistant cordaitaleans to maintain productivity and avoid loss of stem carbon *Paleo-BGC+* as compared to in *Paleo-BGC*.

Discussion

Plant hydraulics in *Paleo-BGC+*

To allow functional comparison across deep time, we based our preliminary xylem morphological characterization of plant fossils on techniques developed for extant plants and included data for two extant eudicots (Hacke et al., 2006). The vulnerability of fossil plant types simulated here was impacted by our choice of contact fraction ($F_c = 0.25$). While it is in the range of contact fractions reported for vessel-bearing angiosperms (Wheeler et al., 2005; Hacke et al., 2006), this choice of F_c may be conservative for some fossil plant types. Plant taxa with a substantial proportion of their sapwood consisting of scalariform tracheids, such as lycopsid secondary xylem or tree fern metaxylem, may have a contact fraction as high as 1. Even in taxa whose secondary xylem lacks scalariform pits but contains, instead, numerous circular-bordered pits, such as medullosans and extinct sphenophytes, contact fraction values may approach 1. In these cases, Carboniferous medullosans, lycopsids and tree ferns—and other taxa that are ecologically important but not modeled here—would be considerably more vulnerable to sapwood dysfunction than estimated in this study. Directly measuring this parameter in fossil plants is challenging: there is little information available on the contact fraction in Carboniferous xylem contact fraction because transverse thin sections and macerations, two common modes of fossil xylem study, do not contain entire tracheids, and radial and transverse sections receive comparatively little attention (Cichan and Taylor, 1984; Wilson et al., 2008, 2015; Wilson and Knoll, 2010; Wilson and Fischer, 2011; Wilson, 2013). Future sensitivity analysis and direct study of fossil plant anatomy will clarify the possible differences in contact fraction of these fossil plant types. Nonetheless, setting a standard F_c allowed analysis of the influence of the xylem traits on vulnerability to sapwood dysfunction.

Due to the fragmentary nature of plant fossils and the preliminary nature of the current dataset, we characterized xylem morphology without respect to its plant part of origin (e.g., bole or branch). However, xylem is not the same in every part of the plant. Increasingly negative water potential in xylem with tree height is mirrored by decreasing conduit

width in many modern tree taxa (Anfodillo et al., 2013; Koçillari et al., 2021). Alternatively, branch and petiole sapwood in some modern tree species is thought to be more vulnerable to cavitation due to a lack of ‘hydraulic oversupply’ in conductive tissue compared to the stem (Cardoso et al., 2020). We therefore designate our physiological inferences (i.e., Ψ_c) as petiolar or ‘near-leaf’ to be conservative of plant function. Additionally, Paleozoic arborescent plants that suffered from vulnerable near-leaf xylem, and were not able to re-translocate nutrients and shed leaves and branches during times of water stress (i.e., not deciduous), may have been at a disadvantage—for example, the medullosans. On the other hand, this would not have been an ecophysiological challenge for Carboniferous cordaitaleans (Looy, 2013), further distinguishing them as a carbon efficient plant type. It is not clear whether these patterns are universal or limited to certain lineages—whether they are adaptive or the result of evolutionary or developmental constraints. Nonetheless, morphological heterogeneity in plant hydraulic pathways may change modeling outcomes for Paleozoic plants, and more detailed fossil information will be required to evaluate this possibility.

While challenges remain in the physiological characterization of extinct-plant hydraulic pathways, our results suggest that the broad morphological differences among extinct plant groups (i.e., vulnerable vs. resistant taxa) and between extinct and extant plants result in physiological differences. Fossil tracheids were shorter and wider than eudicot vessels (Table 1). Despite these differences in proportion, the non-linear relationship between tracheid diameter (D) and tracheid surface area (A_t) in the context of the eudicot-based structure-functional relationship used here (Hacke et al., 2007) produced comparable estimates of mean cavitation water potentials ($\bar{\Psi}_c$) for fossil tracheids and eudicot vessels (but see section “The whole plant perspective: Modern and Paleozoic” below). Even based on this conservative estimate, the addition of sapwood dysfunction had physiological impacts that are relevant to several fields. Reduced stomatal conductance and slowed water use in vulnerable taxa may impact paleo-atmospheric reconstruction (see section “Sapwood dysfunction and stomatal conductance: Is g_{max} really g_{max} ?”), application of forestry principles to ancient ecosystems (see section “Sapwood dysfunction, plant growth and allometry”), regional hydrologic reconstructions (see section “Hydrologic effects of sapwood dysfunction”), and paleoecology of extinct plants broadly.

Sapwood dysfunction and stomatal conductance: Is g_{max} really g_{max} ?

To our knowledge, this is the first attempt to mechanistically predict a functional relationship between sapwood vulnerability to dysfunction and stomatal conductance in a paleo-ecosystem model (see De Kauwe et al., 2014 for comparison to similar

TABLE 4 Final year simulation mean leaf area index (LAI, $m^2 m^{-2}$) and vegetation biomass (mass C m^{-2}) simulated using *Paleo-BGC* (first of each column-pair) and the change in each value when sapwood physiological limitation is added (*Paleo-BGC+*, second of each column-pair, italicized).

Plant type	LAI($m^2 m^{-2}$)	Leaf($g C m^{-2}$)	Stem($kg C m^{-2}$)	Root($kg C m^{-2}$)				
Glacial								
Lycopsid	3.5	<i>-0.4</i>	146.7	<i>-17.7</i>	51.1	<i>-4.8</i>	15.5	<i>-1.5</i>
Medullosan	2.2	<i>-1.1</i>	78.4	<i>-40.0</i>	60.3	<i>-35.2</i>	18.2	<i>-10.6</i>
Tree Fern	4.3	<i>-0.3</i>	126.6	<i>-8.1</i>	46.0	<i>-3.4</i>	13.9	<i>-1.0</i>
Cordaitalean	3.7	<i>-0.2</i>	159.2	<i>-7.8</i>	55.2	<i>46.8</i>	16.7	<i>14.0</i>
EBF-V	1.5	<i>-0.8</i>	122.0	<i>-68.2</i>	82.1	<i>-63.9</i>	24.8	<i>-19.3</i>
EBF-R	1.5	<i>-0.2</i>	122.0	<i>-13.8</i>	82.1	<i>-9.1</i>	24.8	<i>-2.8</i>
Interglacial								
Lycopsid	4.0	<i>0.0</i>	168.0	<i>-0.4</i>	130.9	<i>-4.3</i>	39.4	<i>-1.3</i>
Medullosan	3.3	<i>-1.9</i>	118.4	<i>-69.8</i>	92.4	<i>-57.1</i>	27.8	<i>-17.2</i>
Tree Fern	5.2	<i>0.1</i>	153.0	<i>1.5</i>	117.6	<i>-28.3</i>	35.4	<i>-8.5</i>
Cordaitalean	4.0	<i>0.0</i>	171.7	<i>-1.2</i>	136.7	<i>-5.6</i>	41.2	<i>-1.7</i>
EBF-V	2.1	<i>-0.5</i>	173.0	<i>-45.3</i>	143.0	<i>-70.1</i>	43.0	<i>-21.0</i>
EBF-R	2.1	<i>0.0</i>	173.0	<i>0.4</i>	143.0	<i>-3.6</i>	43.0	<i>-1.0</i>

Adding sapwood limitation generally reduced LAI and biomass (red cells 10% or greater reduction), with a few exceptions in more resistant plant types (green cells increased more than 10%). Simulations were run using two meteorological data sets for Glacial and Interglacial extremes of the Pennsylvanian, with atmospheric CO_2 (182 and 546 ppm), $pO_2 = 28\%$, and each of four fossil plant types and one extant plant type.

models). In resistant plant types, simulated leaf water potentials did not induce sapwood dysfunction (i.e., either by embolism or sapwood allometric deficit), or reduce stomatal conductance (cordaitaleans: Table 2, Figure 6, green line, and Figure 8, m_{sw}). Vulnerable plant types, on the other hand, had stomatal conductance reduced by as much as 82% on average by sapwood dysfunction (Glacial medullosan, Table 2, Figure 6, orange line, and Figure 8, m_{sw}). In *Paleo-BGC+*, air-seeding and embolism (PLC) are the initial cause of sapwood dysfunction. Prolonged embolism also increased simulated sapwood turnover, and altered the allometry of conductive sapwood to supply the canopy with water, which is captured as a proportional cap on stomatal conductance ($g_{s,max}^*$, Table 2, Figure 6, dotted line, and Figure 8).

This major reduction of stomatal conductance of vulnerable plant types in *Paleo-BGC+* implies that the other modes of stomatal-conductance-reduction from its theoretical maximum ($g_{s,max}$; White et al., 2020) were not sufficiently sensitive to prevent simulated sapwood dysfunction for those plant types. This may be due to non-representative parameterization or functional traits missing from the representation of stomata behavior for some extinct plant types. Some stomatal traits may not be accessible using structure-function approaches based on plant fossils, and are unresolved in modern plant physiology, making their use untenable in ecosystem models (e.g., accelerated stomatal responses due to hormone signaling in seed plants; McAdam and Brodribb, 2015, 2016; Cai et al., 2017; Hōrak et al., 2017; Susmilch et al., 2017). Generally, however, more work is needed to elucidate the mechanisms resulting in the broad diversity of relationships between theoretical maximum stomatal conductance to operational

stomatal conductance (McElwain et al., 2016; Clark et al., 2022). Nonetheless, the original *Paleo-BGC* parameters (White et al., 2000) represent the average of modern biome-scale properties, including angiosperms. Stomata are modeled as susceptible to multiple environmental stresses (Jarvis, 1976; Thornton et al., 2002; White et al., 2020). The stomatal conductance reduction simulated in *Paleo-BGC+* represents a conservative approximation of physiological limitation due to sapwood dysfunction. Adding mechanisms to further slow stomatal responses in pursuit of representing Carboniferous plant types (i.e., excluding angiosperm traits like guard cell ABA synthesis or barbell-shaped stomata; Brodribb et al., 2017; Susmilch et al., 2017; Clark et al., 2022), could only exacerbate simulated sapwood dysfunction in this model. In the absence of definitive representations of stomatal function, however, further discussion of these modeling may be framed in terms of a hydraulic safety margin from embolism—defined here as the difference between the average cavitation water potential (Ψ_c , Table 1) and yearly average of minimum petiolar water potentials (Figure 5 and Supplementary Figure 3)—where the stomatal responses are similar but xylem hydraulic limitation varies.

Hydraulic safety margins in *Paleo-BGC+* are largely driven by the relationship between the leaf wilting point, which is prescribed at -2.5 MPa as in the previously published model (White et al., 2020), and the PLC(Ψ_{leaf}) curve for each plant type (see red stars in Figures 4, 5). For example, medullosans had a Ψ_c greater than -2.5 MPa (Table 1). Due to the interaction of these model components, vulnerable plants continued to use water when Ψ_{leaf} was below Ψ_c , despite having already sustained 50% loss of sapwood conductivity or

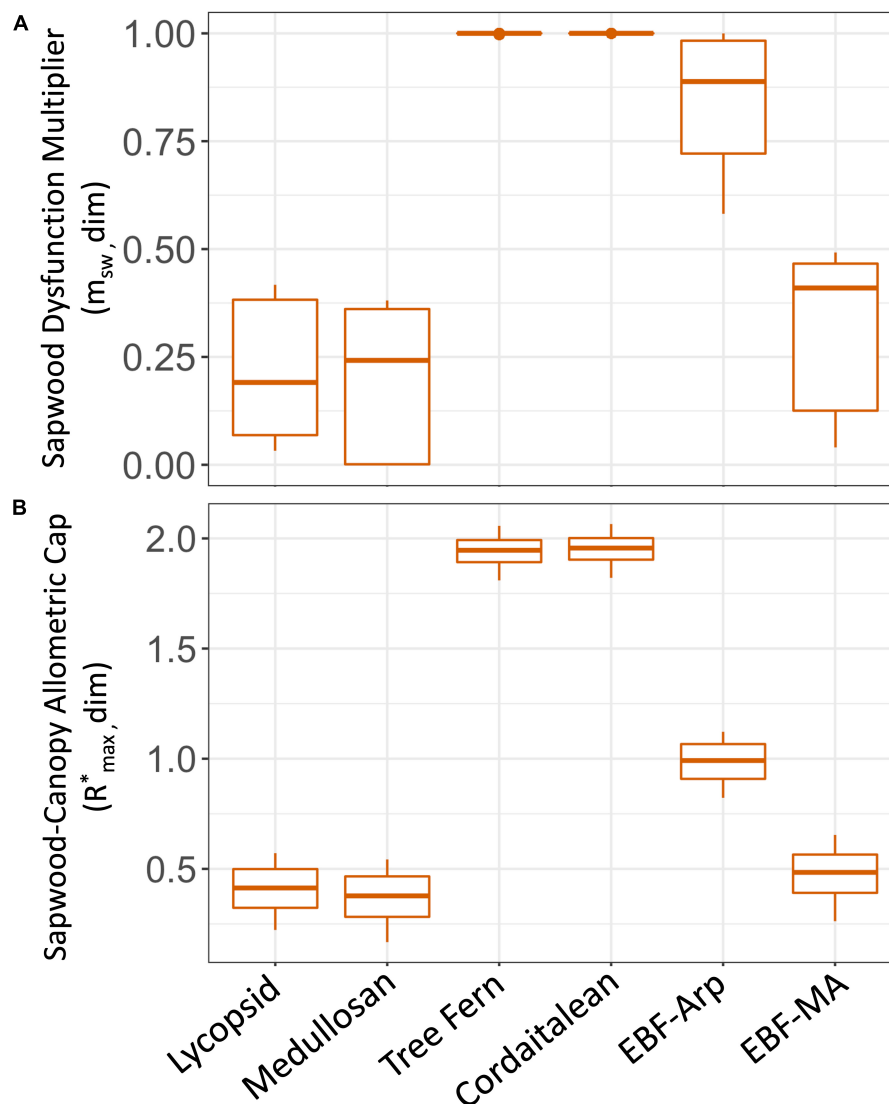


FIGURE 8

Simulated sapwood dysfunction responses as represented in *Paleo-BGC+*. **(A)** Scalar multiplier (m_{sw}) used to reduce stomatal conductance in proportion to loss of xylem conductivity due to air seeding, embolism, and cavitation. **(B)** Standing biomass allometry as a proportion of assumed sufficient sapwood allometry (R^*_{max}) used to place an upper limit on stomatal conductance ($g^*_{s,max} = R^*_{max} g_{s,max}$). Higher values Boxplot centerline are simulation medians, top and bottom of boxes are first and third quartile, whiskers extend to include outliers, at most to the 150% of the interquartile range.

more (Figure 5 and Supplementary Figure 3). This resulted in a negative safety margin (Table 5), which may imply an anisohydric water use strategy (Skelton et al., 2015). Further, medullosans lose a large proportion of functional sapwood each year, and under these environmental conditions have at most 57% of the sapwood required to support maximum canopy conductance (Table 2 and Figure 6, dotted line, and see section “Discussion”). With the addition of sapwood dysfunction, medullosans experience less extreme leaf water potentials in both climate scenarios, as compared to in *Paleo-BGC* (Figure 5), similar to plants with imposed loss of sapwood conductivity

under well-watered conditions (Hubbard et al., 2001). Sapwood dysfunction resistant plant types, such as cordaitaleans and tree ferns, closed stomata due to loss of leaf turgor before any appreciable xylem embolism occurs, allowing the maintenance of sufficient sapwood to support maximum canopy conductance from year to year (Figure 5 and Supplementary Figure 3) as is the case with many modern tropical trees.

Simulated hydraulic safety, and more generally sapwood-canopy coordination, points toward a theoretical basis for reducing the nuisance variability in the relationship between the fossil-estimable $g_{s,max}$ and operational stomatal conductance

TABLE 5 Simulated hydraulic safety margin from embolism for four extinct plant types using *Paleo-BGC* (White et al., 2020) under tropical sub-humid conditions.

Plant type	Safety margin ($\bar{\Psi}_C - \Psi_{Min}$; MPa)	
	Glacial	Interglacial
Lycopsid	-0.5	-0.6
Medullosan	-0.8	-0.8
Tree Fern	1.1	0.9
Cordaitalean	3.7	3.5

Safety margins are the difference between the average cavitation water potential ($\bar{\Psi}_C$, Table 1) and yearly average of minimum petiolar water potentials (Ψ_{min} , Figure 5 and Supplementary Figure 3). Simulations were run using two meteorological data sets for Glacial and Interglacial extremes of the Pennsylvanian, with atmospheric CO₂ (182 and 546 ppm), pO₂ = 28%.

($g_{s,op}$; McElwain et al., 2016). Such a clarification would be favorable in the use of plant fossil traits in paleo-climatology (Franks and Beerling, 2009), as well as paleo-ecosystem modeling efforts (White et al., 2020; Wilson et al., 2020; Matthaeus et al., 2021; Richey et al., 2021). In particular, regardless of stomatal size and density, transpiration induced plant water potential that exceeds xylem tolerances will result in embolism. For some plant types, embolism limits water supply to leaves, reducing stomatal conductance and transpiration (i.e., reduced $g_{s,op}$ despite high $g_{s,max}$; lycopsids and medullosans in Figure 7). Missing from our current approach is the consideration of stem traits like hydraulic capacitance (Meinzer et al., 2008, 2009), and whole-plant traits like hydraulic segmentation and oversupply (Cardoso et al., 2020; Song et al., 2022), which may help vulnerable plant types avoid loss of function due to embolism. Addressing these traits in future efforts should further clarify the relationship between $g_{s,max}$ and $g_{s,op}$, improving the utility of leaf fossils for paleo-climate and pale-ecosystem science.

Sapwood dysfunction, plant growth and allometry

We have implemented a single functional relationship between simulated environment and sapwood turnover through the proxy of fossil-informed xylem cavitation-induced embolism in *Paleo-BGC+*. This functional relationship does not consider possible feedbacks to leaf water status and viability, such as runaway cavitation-induced embolism (Tyree and Sperry, 1988), the additional C cost of actively replacing lost tissues, or the hydraulic protective effect that may be gained by accumulating excess sapwood (Delucia et al., 2001; Cardoso et al., 2020). Further, slowed plant water in the absence of resource competition (i.e., as *Paleo-BGC* simulates monotypic stands) also extended the growing season for vulnerable plants, buffering the effects of sapwood dysfunction growth (Figure 5 and Supplementary Figure 2). Nonetheless, adding this

functional relationship that considers only the direct impacts of cavitation-induced embolism to *Paleo-BGC* resulted differences in absolute biomass, and biomass allometry between different taxa (Table 4 and Supplementary Figure 5).

Considerable biomass differences accumulated between plant types due to sapwood dysfunction over 50 years of simulation time. In the last year of simulation, the vulnerable plant types (medullosans and EBF-V) were reduced in LAI, and Leaf, Stem and Root C by 50% or more in *Paleo-BGC+* as compared to *Paleo-BGC* (Table 4). This reduction is due to the severe curtailing of stomatal conductance due to our new sapwood dysfunction scalar, m_{sw} , based on xylem embolism (Figures 6, 8) and accumulated sapwood allometric deficit (R^*_{max} , Figures 6, 8). For vulnerable plant types, percent loss of conductivity (PLC) decreases m_{sw} directly, while increased sapwood turnover rate increases in proportion to PLC, inducing a deficit of C in sapwood relative to canopy. Reductions in absolute stem C in vulnerable plant types result from the interaction of overall reduced assimilation and increased sapwood turnover, each of which feeds back into further reducing assimilation via reduced LAI and the standing proportion of assumed sufficient sapwood allometry (R^*_{max}) respectively. On the other hand, Glacial scenario cordaitaleans had increased stem and root C with *Paleo-BGC+* compared to *Paleo-BGC*. Cordaitalean stomatal conductance was not reduced by m_{sw} (Figure 8), as their simulated PLC values did not increase above zero based on the water potentials simulated by *Paleo-BGC+* (Figures 4, 5). Further, dynamic sapwood turnover rates were decreased from the default value, promoting biomass accumulation. This potential for stem and root biomass accumulation may help explain the giant stature of some cordaitalean trees during the Carboniferous Period (Falcon-Lang and Bashforth, 2005), may have provided a hydraulic buffer to canopy conductance under high evaporation environments (Delucia et al., 2001; Cardoso et al., 2020), or simply allowed cordaitaleans to use assimilated carbon more efficiently.

In *Paleo-BGC* and *Paleo-BGC+*, the standing biomass allometry of canopy to sapwood ($C_L:C_{SW}$) is a product of allocation and turnover of both canopy and sapwood. Further, allocation and turnover may each be influenced by the environment in these models, and in modern taxa: for example, plant available nitrogen and water (Callaway et al., 1994) or vapor pressure deficit (Delucia et al., 2001). Among modern taxa, trees increase the ratio of sapwood to canopy area in drier environments, while other taxa are unchanged (Delucia et al., 2001). However, the interaction of xylem embolism with allocation/turnover in sapwood and scaling to the canopy, is unclear. Therefore, it is not clear whether observed differences in $C_L:C_{SW}$ (or analogous allometries based on other quantities, i.e., area or volume) among environments and, or taxa are the result of changes to allocation, turnover, or both (Callaway et al., 1994; Delucia et al., 2001). For example, decreases in standing $C_L:C_{SW}$

in dry environments may be the result of increased leaf turnover, an increase in sapwood allocation relative to canopy allocation, or both. The modes of plant allometric response to sapwood dysfunction may be clarified with experiments considering changes to quantity and embolism-status of sapwood, and quantity and water status of canopy.

Hydrologic effects of sapwood dysfunction

Slowed water use as a result of sapwood dysfunction increased mean surface discharge runoff in both scenarios, for vulnerable plant types (model comparisons summarized in [Table 6](#)). Following ([White et al., 2020](#)), we examine the effect of sapwood dysfunction on surface runoff at a spatial scale with relevance to today's world. The African Congo River basin experiences similar conditions to those in our Pennsylvanian meteorological data. With an annual precipitation of 150–200 cm yr⁻¹ across 4 × 10⁶ km² ([Munzimi et al., 2015](#)), the Congo exports 1457 km³ yr⁻¹ of water to the Atlantic Ocean of ([Runge, 2007](#)). For comparison, we use our high atmospheric CO₂ meteorology (546 ppm), which is comparable in precipitation to that used in [White et al. \(2020\)](#), and to the Congo basin ([Table 2](#)). A Congo basin covered in lycopsids would produce 963 km³ yr⁻¹ of water discharge using *Paleo*-BGC compared to 2333 km³ yr⁻¹ using *Paleo*-BGC + with sapwood dysfunction added. This increase in water output is due to the slowing of water use by lycopsids and their reduced leaf area index (LAI, [Table 4](#) and [Figure 7](#)). A Congo basin covered in tree ferns, on the other hand, would change little due to sapwood dysfunction (*Paleo*-BGC: 2963 km³ yr⁻¹, *Paleo*-BGC + : 2951 km³ yr⁻¹). The addition of a stem-functional feedback brings the water use of Mississippian and early Pennsylvanian dominant lycopsids closer to that of their late Pennsylvanian replacement, the Marattialean tree ferns (but see section “Discussion”). Further, adding this representation of sapwood-dysfunction-limited transpiration reverses the prediction made in [White et al. \(2020\)](#) for this paleo-location, and suggests that overall Carboniferous plants would allow more runoff.

The whole plant perspective: Modern and Paleozoic

Several of the Carboniferous plant types studied here have non-analog tracheids. In particular, lycopsids and medullosans have the widest conducting cells considered in this study ([Table 1](#)), despite being short compared to multicellular vessels. Lycopsids and medullosans have been proposed to be fast users of water due to their foliar characteristics ([Wilson, 2013](#); [Wilson et al., 2015, 2020](#); [White et al., 2020](#)). Presumably,

their wide conducting cells represent an adaptation to improve maximum xylem hydraulic conductivity in the context of being evolutionarily limited to tracheids. This strategy may have allowed for fast growth in everwet conditions, when soil water potential never dropped below critical cavitation potentials. However, in the seasonally wet environment used for our simulations ([Table 3](#) and [Supplementary Figure 1](#)), the same traits that might confer high sapwood conductance, caused sapwood dysfunction in lycopsids and medullosans. This result further confirms the importance of moisture seasonality, and microhabitat in shaping the evolutionary trajectory of plant clades, and to biome turnover in the Carboniferous ([DiMichele, 2014](#); [Wilson et al., 2017](#)).

Our results show the direct cost of wider tracheids on assimilation due to air seeding and loss of sapwood function. However wide conducting cells, such as those found in lycopsids and medullosans, have additional costs that long conducting cells may not ([Wilson et al., 2008](#); [Wilson and Fischer, 2011](#); [Wilson, 2013](#)). Wide tracheids have reduced structural stability and may suffer irreversible damage (e.g., implosion) more easily, or require additional carbon costs to reinforce their secondary wall ([Sperry et al., 2016](#); [Koçillari et al., 2021](#)). Additionally, wide tracheids refill less readily under near-zero soil water potentials ([Yang and Tyree, 1992](#)), and may allow embolism to spread more rapidly due to air-water meniscus geometry ([Venturas et al., 2017](#)).

Our results suggests that medullosans were particularly affected by the vulnerability of their wide tracheids (average diameter 165 μm), due to sapwood dysfunction. In particular, medullosans lost a large proportion of sapwood to turnover each dry season in *Paleo*-BGC +. In modern trees this would cause leaves to be damaged due to lack of water supply ([Holloway-Phillips, 2020](#)). This could suggest facultative deciduousness in medullosans that would have resulted in a large carbon cost as a result of losing and regrowing large leaves frequently. It may be that this ‘carbon inefficiency’ in combination with a carbon intensive reproductive strategy (i.e., large seeds) limited the survival and reproduction of the largest-tracheid-medullosans to everwet environments as previously hypothesized by [Wilson et al., 2008, 2015](#) and [Wilson \(2013\)](#) based on modeled hydraulic parameters. Simulated physiology based on fossil morphology, therefore, might be used to explain why certain medullosans lineages persisted into the Permian while others disappeared near the end of Carboniferous.

In contrast to medullosans, our results suggest that the late Pennsylvanian dominant Marattialean tree ferns were resistant to sapwood dysfunction with some climate seasonality. These tree ferns do not have ‘true’ secondary xylem, rather, they have vascular bundles in the stem, and the actinostele in adventitious roots that have a mix of wide metaxylem tracheids (average diameter 75 μm) and considerably narrower protoxylem tracheids (10–20 μm diameter). This apparent bimodal distribution of tracheid diameters may have served a

TABLE 6 Overview of changes in ecosystem modeling outcomes using *Paleo-BGC +* (with sapwood dysfunction) as compared to the previously published version of the model.

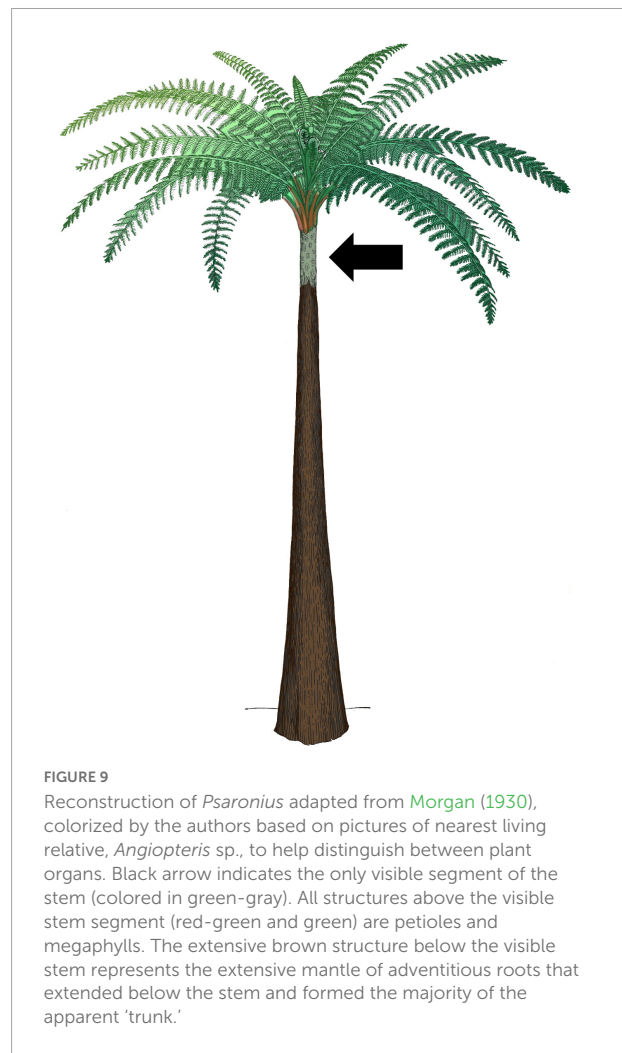
Scenario	Water potential	Transpiration	Canopy	Stem/Root	Stream flow	N cycle
Vulnerable	+	-	-	-	+	±
Resistant				+		

Ecosystem effects of sapwood effects vary by plant type and conditions. Overview combines conditions from Glacial and Interglacial scenarios in a seasonally dry tropical location, from GENESIS v3 simulations of the Pennsylvanian Period. Plant types are differentiated by modeled xylem cavitation and sapwood allometric limitation of stomatal conductance and productivity, that is, as vulnerable (lycopoid and medullosans; low m_{SW} and R^*_{max}) or resistant (cordaitalean and tree ferns; high m_{SW} and R^*_{max}) to sapwood dysfunction based on xylem fossil anatomy. Green cells (+) indicate an increased outcome, and red cells (-) indicate a decrease. Empty cells indicate no change. Water potential represents both leaf and soil. Transpiration is represented by stomatal conductance. Canopy outcomes are leaf area index (LAI) and leaf C. Nitrogen cycle fluxes are N mineralization and leaching; details are present in the [Supplementary materials](#).

similar function to tracheid-embedded vessels in some modern dicot woods (Carlquist, 2009). In tree ferns, smaller protoxylem tracheids may have maintained xylem conductivity through dry periods and water potentials that would embolize larger metaxylem tracheids.

Particularly in the roots, this xylem morphological paradigm may have allowed the Marratialean tree fern *Psaronius* (Figure 9) to supply developing fiddleheads with water before sufficient stem and leaf xylem had grown to supply their fully developed form. This may be analogous to the function of narrow latewood conduits in some modern temperate taxa that support subsequent year leaf flush when wide earlywood conduits have been embolized (White, 1992; Gullo et al., 1995; Yin et al., 2016). Interestingly, this strategy may have ceased to be viable as seasonally humid tropics became arid at the Permo-Carboniferous boundary, when Marratialean tree ferns were replaced by coniferophytes like the cordaitaleans (Wilson et al., 2017).

Cordaitaleans and other related conifers of the Permo-Carboniferous periods have several traits that likely protected them from environmental variability. Morphologically, they are predicted to have the most cavitation resistant xylem (Table 1 and Figures 2, 4, 8; Wilson, 2013). According to our model, cordaitaleans also avoided sapwood turnover that facilitated higher biomass accumulation, particularly in the glacial climate scenario. This is interesting because narrow tracheids are also protective of enhanced cavitation due to freeze thaw-cycles (Pittermann and Sperry, 2003, 2006), which were likely more widespread in the colder, glacial parts of the Carboniferous (Matthaeus et al., 2021). Besides xylem traits, Carboniferous cordaitaleans and conifers reproduced using seeds. Seed dormancy, in particular, is thought to have evolved to promote reproductive success in the context of environmental variability (Willis et al., 2014). The earliest seeds showing evidence of quiescence are found in a Permo-Carboniferous conifer (Mapes et al., 1989). It may be that cordaitalean and conifer sapwood morphology that was resistant to dysfunction, coupled with seeds, allowed them to persist and diversify through Permo-Carboniferous aridification, while medullosan pteridosperms diversity dropped.



Taken together, these results from *Paleo-BGC +* modeling of extinct plants with fossilized anatomy provides novel context to ongoing research on the cavitation resistance and physiological resilience of non-angiosperm vascular plants, particularly ferns. Recent research has shown that ferns are capable of extreme resilience to drought stress (Watkins et al., 2010; Pittermann et al., 2011; Baer et al., 2016, 2020; Holmlund et al., 2016). This

resilience is enabled by a diverse suite of mechanisms of stress recovery and embolism protection, including: root pressure (Holmlund et al., 2020); anatomical adaptations, including endodermal layers and the presence of pectin in the primary xylem (Holmlund et al., 2019); employing a broad range of xylem cell sizes (Pittermann et al., 2011); and novel connectivity of xylem strands at the organ scale (Brodersen et al., 2012; Suissa and Friedman, 2021) and at the individual xylem cell scale (Pittermann et al., 2011; Brodersen et al., 2014). Results from *Psaronius* suggest that it may have occupied an ecological niche presently occupied by many ferns (e.g., *Dryopteris arguta*, coastal wood fern; Watkins et al., 2010; Pittermann et al., 2011; Baer et al., 2016; Holmlund et al., 2016) and, also, that any of these adaptations, if they were present, would have further enhanced drought resistance and stress recovery in these early tree ferns.

Cordaitaleans, related conifers, and the medullosans present an additional challenge because of their large morphological differences from existing seed plant lineages, specifically the broad leaves in cordaitaleans and the large fronds, anastomosing stem vascular bundles, and large tracheids in *Medullosa* (Wilson, 2013). Despite these challenges, the modeled results for the cordaitaleans and coniferophytes presented here are in broad accord with cavitation vulnerability curves measured from riparian conifers (Pittermann et al., 2006). Furthermore, medullosan vulnerability to cavitation induced embolism is only marginally greater than that measured from the extant tree fern *Dicksonia antarctica* (Pittermann et al., 2011), which has maximum conduit diameters less than one-third as wide as *Medullosa's* xylem cells, suggesting that medullosan modeled vulnerability may be a conservative estimate. Finally, although there is not yet a way to identify some of the specialized drought resistance adaptations identified in ferns (e.g., root pressure, pectin in xylem) from fossilized stems, the multi-million-year persistence of all the extinct lineages presented here, through many drought events, suggests that similar adaptations may have arisen by the Permo-Carboniferous periods.

This research shows that focusing on a single plant organ or functional trait limits understanding plant water use, especially in the context of changing climates and atmospheric conditions. Further, this work supports an ecomorphic functional definition of plant types that supports further fossil-informed ecosystem modeling. In addition, future modeling should consider the whole plant including the complexity of hydraulic pathway morphology (e.g., in *Psaronius*) together with the carbon economy (e.g., reproductive costs in cordaitaleans/medullosans). However, additional high-quality fossil information is needed to contribute to both model development and accuracy.

Finally, this work indicates that simulation of plants, particularly in deep-time, should not be considered outside of their evolutionary and developmental contexts. For example,

large leaves, such as those found in tree ferns and medullosans, may have been promoted by cold, low CO₂ conditions, and subsequently been maladaptive in hot, high CO₂ conditions (Sack and Holbrook, 2006). The subsequent persistence, or disappearance of those lineages may be due to differences in another part of their hydraulic pathway (such as the tree ferns). Alternatively, seeds may have promoted the persistence of carbon efficient plant types, such as the cordaitaleans, or been a burden for those that were already carbon stressed associated with vulnerable hydraulic systems, such as the medullosans.

Conclusion

Sapwood dysfunction reduced simulated plant water use in some Carboniferous plant types, despite those taxa having high maximum stomatal conductance. Simulations that include both leaf and stem conductivity better resolve the survivability of ancient taxa with regard to climate changes and help support certain plant-turnover events, such as the lycopsids' replacement by tree ferns, within the tropical forests during the late Pennsylvanian (DiMichele, 2014; Wilson et al., 2017).

We also found that direct reduction of assimilation by sapwood dysfunction under seasonal moisture regimes may largely explain the disappearance of medullosan pteridosperms in the Pennsylvanian tropics. This is particularly likely when the overall high construction cost of Pennsylvanian medullosans is considered (DiMichele et al., 2006). However, sapwood dysfunction alone does not explain the relegation of lycopsids to subdominants in the late Pennsylvanian. Rather, we suggest that tree ferns may have out-competed lycopsids in seasonally dry areas by quickly resuming productivity after drought by virtue of the 'division of labor' between tree ferns' resistant protoxylem and vulnerable metaxylem (DiMichele et al., 2002). In contrast, our results support the importance of cordaitalean and early conifer carbon efficiency resulting from cavitation resistant sapwood. These traits may have led to their dominance in the early Permian and may have enhanced cooling across the Permo-Carboniferous boundary (Chen et al., 2021).

Sapwood dysfunction, and sapwood-canopy coordination are plant properties that have the potential to impact Earth system processes. The effects of sapwood dysfunction, however, must be better integrated into future modeling efforts to represent leaf water status compromise, canopy loss, and additional C costs of tissue replacement in the canopy and sapwood. These issues have been given a water-stress-limited treatment for modern plants in Community Land Model 5 (Kennedy et al., 2019). Additional development is needed to apply modern Earth system process simulations to extinct plant types due to the likely non-analog canopy and stem trait coordination seen in our results. Future empirical and theoretical development of these concepts will allow us to better

predict the responses of vegetation to past and future climate change.

Data availability statement

The datasets presented in this study can be found in online repositories. The names of the repository/repositories and accession number(s) can be found below: <https://zenodo.org/record/6588761> and <https://doi.org/10.5281/zenodo.6588761>.

Author contributions

WM, JPW, and JDW established the model background and designed the research plan. WM implemented the model, performed the simulations, and drafted the initial manuscript. WM, JPW, JM, IM, and JDW contributed to development of figures and manuscript text. All authors contributed to the article and approved the submitted version.

Funding

The authors thank the National Science Foundation for its support (EAR-1338247 to JDW), EAR-1338281 (to IM) and thank the European Research Council for its support (ERC-2011-StG and 279962-OXYEVOL to JM).

References

- Alder, J. R., Hostetler, S. W., Pollard, D., and Schmittner, A. (2011). Evaluation of a present-day climate simulation with a new coupled atmosphere-ocean model GENMOM. *Geosci. Model Dev.* 4, 69–83. doi: 10.5194/gmd-4-69-2011
- Anfodillo, T., Petit, G., and Crivellaro, A. (2013). Axial conduit widening in woody species: A still neglected anatomical pattern. *IAWA J.* 34, 352–364. doi: 10.1163/22941932-00000030
- Avila, R. T., Guan, X., Kane, C. N., Cardoso, A. A., Batz, T. A., DaMatta, F. M., et al. (2022). Xylem embolism spread is largely prevented by interconduit pit membranes until the majority of conduits are gas-filled. *Plant Cell Environ.* 45, 1204–1215. doi: 10.1111/pce.14253
- Baer, A., Wheeler, J. K., and Pittermann, J. (2016). Not dead yet: The seasonal water relations of two perennial ferns during California's exceptional drought. *New Phytol.* 210, 122–132. doi: 10.1111/nph.13770
- Baer, A., Wheeler, J. K., and Pittermann, J. (2020). Limited hydraulic adjustments drive the acclimation response of *Pteridium aquilinum* to variable light. *Ann. Bot.* 125, 691–700. doi: 10.1093/aob/mcaa006
- Bashforth, A. R., Cleal, C. J., Gibling, M. R., Falcon-Lang, H. J., and Miller, R. F. (2014). Paleoeology of Early Pennsylvanian vegetation on a seasonally dry tropical landscape (Tynemouth Creek Formation, New Brunswick, Canada). *Rev. Palaeobot. Palynol.* 200, 229–263. doi: 10.1016/j.revpalbo.2013.09.006
- Berling, D. J., and Royer, D. L. (2002). Reading a CO₂ signal from fossil stomata. *New Phytol.* 153, 387–397. doi: 10.1046/j.0028-646X.2001.00335.x
- Boyce, C. K., and Zwieniecki, M. A. (2019). The prospects for constraining productivity through time with the whole-plant physiology of fossils. *New Phytol.* 223, 40–49. doi: 10.1111/nph.15446
- Boyce, C. K., Brodrigg, T. J., Feild, T. S., and Zwieniecki, M. A. (2009). Angiosperm leaf vein evolution was physiologically and environmentally transformative. *Proc. R. Soc. B* 276, 1771–1776. doi: 10.1098/rspb.2008.1919
- Brodersen, C. R., Roark, L. C., and Pittermann, J. (2012). The physiological implications of primary xylem organization in two ferns: Fern xylem and physiology. *Plant Cell Environ.* 35, 1898–1911. doi: 10.1111/j.1365-3040.2012.02524.x
- Brodersen, C., Jansen, S., Choat, B., Rico, C., and Pittermann, J. (2014). Cavitation Resistance in Seedless Vascular Plants: The Structure and Function of Interconduit Pit Membranes. *Plant Physiol.* 165, 895–904. doi: 10.1104/pp.113.226522
- Brodrigg, T. J., and Feild, T. S. (2010). Leaf hydraulic evolution led a surge in leaf photosynthetic capacity during early angiosperm diversification. *Ecol. Lett.* 13, 175–183. doi: 10.1111/j.1461-0248.2009.01410.x
- Brodrigg, T. J., McAdam, S. A., and Carins Murphy, M. R. (2017). Xylem and stomata, coordinated through time and space: Functional linkages between xylem and stomata. *Plant Cell Environ.* 40, 872–880. doi: 10.1111/pce.12817
- Cai, S., Chen, G., Wang, Y., Huang, Y., Marchant, D. B., Wang, Y., et al. (2017). Evolutionary conservation of ABA signaling for stomatal closure. *Plant Physiol.* 174, 732–747. doi: 10.1104/pp.16.01848
- Callaway, R. M., DeLucia, E. H., and Schlesinger, W. H. (1994). Biomass Allocation of Montane and Desert Ponderosa Pine: An Analog for Response to Climate Change. *Ecology* 75, 1474–1481. doi: 10.2307/1937470
- Cardoso, A. A., Batz, T. A., and McAdam, S. A. M. (2020). Xylem Embolism Resistance Determines Leaf Mortality during Drought in *Persea americana*. *Plant Physiol.* 182, 547–554. doi: 10.1104/pp.19.00585

Acknowledgments

We thank Christopher J. Poulsen and Michael T. Hren for their support of past work leading to this manuscript.

Conflict of interest

The authors declare that the research was conducted in the absence of any commercial or financial relationships that could be construed as a potential conflict of interest.

Publisher's note

All claims expressed in this article are solely those of the authors and do not necessarily represent those of their affiliated organizations, or those of the publisher, the editors and the reviewers. Any product that may be evaluated in this article, or claim that may be made by its manufacturer, is not guaranteed or endorsed by the publisher.

Supplementary material

The Supplementary Material for this article can be found online at: <https://www.frontiersin.org/articles/10.3389/fevo.2022.955066/full#supplementary-material>

- Carlquist, S. (2009). Non-random Vessel Distribution in Woods: Patterns, Modes, Diversity, Correlations. *Aliso* 27, 39–58. doi: 10.5642/aliso.20092701.04
- Chattaway, M. M. (1952). The sapwood-heartwood transition. *Australian Forestry* 16, 25–34. doi: 10.1080/00049158.1952.10675284
- Chen, B., Chen, J., Qie, W., Huang, P., He, T., and Joachimski, M. M. (2021). Was climatic cooling during the earliest Carboniferous driven by expansion of seed plants? *Earth Planetary Sci. Lett.* 7:116953. doi: 10.1016/j.epsl.2021.116953
- Choat, B., Jansen, S., Brodribb, T. J., Cochard, H., Delzon, S., Bhaskar, R., et al. (2012). Global convergence in the vulnerability of forests to drought. *Nature* 491, 752–755. doi: 10.1038/nature11688
- Christman, M. A., Sperry, J. S., and Smith, D. D. (2012). Rare pits, large vessels and extreme vulnerability to cavitation in a ring-porous tree species. *New Phytol.* 193, 713–720. doi: 10.1111/j.1469-8137.2011.03984.x
- Cichan, M. A. (1985). Vascular Cambium and Wood Development in Carboniferous Plants. I. Lepidodendrales. *Am. J. Bot.* 72, 1163–1176. doi: 10.1002/j.1537-2197.1985.tb08369.x
- Cichan, M. A. (1986). Conductance in the wood of selected Carboniferous plants. *Paleobiology* 12, 302–310. doi: 10.1017/S0094837300013804
- Cichan, M. A., and Taylor, T. N. (1984). A Method for Determining Tracheid Lengths in Petrified Wood by Analysis of Cross Sections. *Ann. Bot.* 53, 219–226. doi: 10.1093/oxfordjournals.aob.a086683
- Clark, J. W., Harris, B. J., Hetherington, A. J., Hurtado-Castano, N., Brench, R. A., Casson, S., et al. (2022). The origin and evolution of stomata. *Curr. Biol.* 32:R539–R553. doi: 10.1016/j.cub.2022.04.040
- De Kauwe, M. G., Medlyn, B. E., Zaehle, S., Walker, A. P., Dietze, M. C., Wang, Y., et al. (2014). Where does the carbon go? A model–data intercomparison of vegetation carbon allocation and turnover processes at two temperate forest free-air CO₂ enrichment sites. *New Phytol.* 203, 883–899. doi: 10.1111/nph.12847
- DeLucia, E. H., Callaway, R. M., and Schlesinger, W. H. (1994). Offsetting changes in biomass allocation and photosynthesis in ponderosa pine (*Pinus ponderosa*) in response to climate change. *Tree Physiol.* 14, 669–677. doi: 10.1093/treephys/14.7-8-9.669
- Delucia, E. H., Maherali, H., and Carey, E. V. (2001). Climate-driven changes in biomass allocation in pines. *Glob. Change Biol.* 6, 587–593. doi: 10.1046/j.1365-2486.2000.00338.x
- De Vries, F. W. T. P. (1975). The cost of maintenance processes in plant cells. *Ann. Bot.* 39, 77–92. doi: 10.1093/oxfordjournals.aob.a084919
- DiMichele, W. A. (2014). Wetland-Dryland Vegetational Dynamics in the Pennsylvanian Ice Age Tropics. *Int. J. Plant Sci.* 175, 123–164. doi: 10.1086/675235
- DiMichele, W. A. I., Montañez, P., Poulsen, C. J., and Tabor, N. J. (2009). Climate and vegetational regime shifts in the late Paleozoic ice age earth. *Geobiology* 7, 200–226. doi: 10.1111/j.1472-4669.2009.00192.x
- DiMichele, W. A., Phillips, T. L., and Nelson, W. J. (2002). Place vs. time and vegetational persistence: A comparison of four tropical mires from the Illinois Basin during the height of the Pennsylvanian Ice Age. *Int. J. Coal Geol.* 50, 43–72. doi: 10.1016/S0166-5162(02)00113-1
- DiMichele, W. A., Phillips, T. L., and Pfefferkorn, H. W. (2006). Paleogeology of Late Paleozoic pteridosperms from tropical Euramerica. *J. Torrey Botanical Soc.* 133, 83–118. doi: 10.3159/1095-5674(2006)133[83:POLPPF]2.0.CO;2
- Domec, J.-C., Warren, J. M., Meinzer, F. C., and Lachenbruch, B. (2009). Safety Factors for Xylem Failure by Implosion and Air-Seeding Within Roots, Trunks and Branches of Young and Old Conifer Trees. *IAWA J.* 30, 101–120. doi: 10.1163/22941932-90000207
- Ewers, F. W. (1985). Xylem Structure and Water Conduction in Conifer Trees, Dicot Trees, and Lianas. *IAWA J.* 6, 309–317. doi: 10.1163/22941932-9000959
- Falcon-Lang, H. J., and Bashforth, A. R. (2004). Pennsylvanian uplands were forested by giant cordaitalean trees. *Geology* 32:417. doi: 10.1130/G20371.1
- Falcon-Lang, H. J., and Bashforth, A. R. (2005). Morphology, anatomy, and upland ecology of large cordaitalean trees from the Middle Pennsylvanian of Newfoundland. *Rev. Palaeobot. Palynol.* 135, 223–243. doi: 10.1016/j.revpalbo.2005.04.001
- Farquhar, G. D., von Caemmerer, S., and Berry, J. A. (1980). A biochemical model of photosynthetic CO₂ assimilation in leaves of C₃ species. *Planta* 149, 78–90. doi: 10.1007/BF00386231
- Finsinger, W., and Wagner-Cremer, F. (2009). Stomatal-based inference models for reconstruction of atmospheric CO₂ concentration: A method assessment using a calibration and validation approach. *Holocene* 19, 757–764. doi: 10.1177/0959683609105300
- Franks, P. J., and Beerling, D. J. (2009). Maximum leaf conductance driven by CO₂ effects on stomatal size and density over geologic time. *Proc. Natl. Acad. Sci. U.S.A.* 106, 10343–10347. doi: 10.1073/pnas.0904209106
- Gough, D. O. (1981). Solar interior structure and luminosity variations. *Phys. Sol. Variations* 74, 21–34. doi: 10.1007/BF00151270
- Gullo, M. A., Salleo, S., Piaceri, E. C., and Rosso, R. (1995). Relations between vulnerability to xylem embolism and xylem conduit dimensions in young trees of *Quercus corris*. *Plant Cell Environ.* 18, 661–669. doi: 10.1111/j.1365-3040.1995.tb00567.x
- Hacke, U. G., Sperry, J. S., Feild, T. S., Sano, Y., Sikkema, E. H., and Pittermann, J. (2007). Water Transport in Vesselless Angiosperms: Conducting Efficiency and Cavitation Safety. *Int. J. Plant Sci.* 168, 1113–1126. doi: 10.1086/520724
- Hacke, U. G., Sperry, J. S., Wheeler, J. K., and Castro, L. (2006). Scaling of angiosperm xylem structure with safety and efficiency. *Tree Physiol.* 26, 689–701. doi: 10.1093/treephys/26.6.689
- Haworth, M., and Raschi, A. (2014). An assessment of the use of epidermal micro-morphological features to estimate leaf economics of Late Triassic–Early Jurassic fossil Ginkgoales. *Rev. Palaeobot. Palynol.* 205, 1–8. doi: 10.1016/j.revpalbo.2014.02.007
- Haworth, M., Gallagher, A., Sum, E., Hill-Donnelly, M., Steinthorsdottir, M., and McElwain, J. (2014). On the reconstruction of plant photosynthetic and stress physiology across the Triassic–Jurassic boundary. *Turkish J. Earth Sci.* 23, 321–329. doi: 10.3906/yer-1202-4
- Holloway-Phillips, M. (2020). Variation in Xylem Resistance to Cavitation Explains Why Some Leaves Within a Canopy Are More Likely to Die under Water Stress. *Plant Physiol.* 182, 450–452. doi: 10.1104/pp.19.01394
- Holmlund, H. I., Davis, S. D., Ewers, F. W., Aguirre, N. M., Sapes, G., Sala, A., et al. (2020). Positive root pressure is critical for whole-plant desiccation recovery in two species of terrestrial resurrection ferns. *J. Exp. Bot.* 71, 1139–1150. doi: 10.1093/jxb/erz472
- Holmlund, H. I., Lekson, V. M., Gillespie, B. M., Nakamatsu, N. A., Burns, A. M., Sauer, K. E., et al. (2016). Seasonal changes in tissue-water relations for eight species of ferns during historic drought in California. *Am. J. Bot.* 103, 1607–1617. doi: 10.3732/ajb.1600167
- Holmlund, H. I., Pratt, R. B., Jacobsen, A. L., Davis, S. D., and Pittermann, J. (2019). High-resolution computed tomography reveals dynamics of desiccation and rehydration in fern petioles of a desiccation-tolerant fern. *New Phytol.* 224, 97–105. doi: 10.1111/nph.16067
- Hörak, H., Kollist, H., and Merilo, E. (2017). Fern Stomatal Responses to ABA and CO₂ Depend on Species and Growth Conditions. *Plant Physiol.* 174, 672–679. doi: 10.1104/pp.17.00120
- Horton, D. E., Poulsen, C. J., and Pollard, D. (2010). Influence of high-latitude vegetation feedbacks on late Palaeozoic glacial cycles. *Nat. Geosci.* 3, 572–577. doi: 10.1038/ngeo922
- Hubbard, R. M., Ryan, M. G., Stiller, V., and Sperry, J. S. (2001). Stomatal conductance and photosynthesis vary linearly with plant hydraulic conductance in ponderosa pine. *Plant Cell Environ.* 24, 113–121. doi: 10.1046/j.1365-3040.2001.00660.x
- Jarvis, P. G. (1976). The Interpretation of the Variations in Leaf Water Potential and Stomatal Conductance Found in Canopies in the Field. *Philosophical. Trans. R. Soc. B* 273:17. doi: 10.1098/rstb.1976.0035
- Jarvis, P. G., and Mcnaughton, K. G. (1986). Stomatal Control of Transpiration: Scaling Up from Leaf to Region. *Adv. Ecol. Res.* 15, 1–49. doi: 10.1016/S0065-2504(08)60119-1
- Jinagool, W. (2015). Genetic Variability of Drought Tolerance of Trees of Agronomic Interest: The Role of Vulnerability to Xylem Cavitation. Aubière: Agricultural Sciences, Université Blaise Pascal Clermont-Ferrand II.
- Kennedy, D., Swenson, S., Oleson, K. W., Lawrence, D. M., Fisher, R., Lola da Costa, A. C., et al. (2019). Implementing Plant Hydraulics in the Community Land Model, Version 5. *J. Adv. Model. Earth Syst.* 11, 485–513. doi: 10.1029/2018MS001500
- Kočillari, L., Olson, M. E., Suweis, S., Rocha, R. P., Lovison, A., Cardin, F., et al. (2021). The Widened Pipe Model of plant hydraulic evolution. *Proc. Natl. Acad. Sci. U.S.A.* 118:e2100314118. doi: 10.1073/pnas.2100314118
- Levionnois, S., Kaack, L., Heuret, P., Abel, N., Ziegler, C., Coste, S., et al. (2022). Pit characters determine drought-induced embolism resistance of leaf xylem across 18 Neotropical tree species. *Plant Physiol.* [Epub ahead of print]. doi: 10.1093/plphys/kiac223
- Looy, C. V. (2013). Natural history of a plant trait: Branch-system abscission in Paleozoic conifers and its environmental, autecological, and ecosystem implications in a fire-prone world. *Paleobiology* 39, 235–252. doi: 10.1666/12030

- Macarewicz, S. (2021). *Modeling Ocean Dynamics and Vegetation-Climate Interactions Under Evolving CO₂ During the Late Paleozoic Ice Age*. Ann Arbor, MI: The University of Michigan
- Mapes, G., Rothwell, G. W., and Haworth, M. T. (1989). Evolution of seed dormancy. *Nature* 337, 645–646. doi: 10.1038/337645a0
- Martini, I. P. (ed.) (1997). *Late Glacial and Postglacial Environmental Changes?: Quaternary, Carboniferous-Permian, and Proterozoic*. Oxford: Oxford University Press.
- Matthaeus, W. J., Macarewicz, S. I., Richey, J. D., Wilson, J. P., McElwain, J. C. I., Montañez, P., et al. (2021). Freeze tolerance influenced forest cover and hydrology during the Pennsylvanian. *Proc. Natl. Acad. Sci. U.S.A.* 118:e2025227118. doi: 10.1073/pnas.2025227118
- Mayr, S., Kartusch, B., and Kikuta, S. (2014). Evidence for Air-Seeding: Watching the Formation of Embolism in Conifer Xylem. *J. Plant Hydraulics* 1:e004. doi: 10.20870/jph.2014.e004
- McAdam, S. A. M., and Brodribb, T. J. (2015). The Evolution of Mechanisms Driving the Stomatal Response to Vapor Pressure Deficit. *Plant Physiol.* 167, 833–843. doi: 10.1104/pp.114.252940
- McAdam, S. A. M., and Brodribb, T. J. (2016). Linking Turgor with ABA Biosynthesis: Implications for Stomatal Responses to Vapor Pressure Deficit across Land Plants. *Plant Physiol.* 171, 2008–2016. doi: 10.1104/pp.16.00380
- McElwain, J. C. (1998). Do fossil plants signal palaeoatmospheric carbon dioxide concentration in the geological past? *Philosophical. Trans. R. Soc. London. Series B* 353, 83–96. doi: 10.1098/rstb.1998.0193
- McElwain, J. C., Yiotis, C., and Lawson, T. (2016). Using modern plant trait relationships between observed and theoretical maximum stomatal conductance and vein density to examine patterns of plant macroevolution. *New Phytol.* 209, 94–103. doi: 10.1111/nph.13579
- Meinzer, F. C., Johnson, D. M., Lachenbruch, B., McCulloh, K. A., and Woodruff, D. R. (2009). Xylem hydraulic safety margins in woody plants: Coordination of stomatal control of xylem tension with hydraulic capacitance. *Funct. Ecol.* 23, 922–930. doi: 10.1111/j.1365-2435.2009.01577.x
- Meinzer, F. C., Woodruff, D. R., Domec, J.-C., Goldstein, G., Campanello, P. I., Gatti, M. G., et al. (2008). Coordination of leaf and stem water transport properties in tropical forest trees. *Oecologia* 156, 31–41. doi: 10.1007/s00442-008-0974-5
- Monteith, J. L. (1965). Evaporation and environment. *Symp. Soc. Exp. Biol.* 19, 205–234.
- Monteith, J. L., and Unsworth, M. H. (2013). *Principles of Environmental Physics: Plants, Animals, and The Atmosphere*, 4th Edn. Amsterdam: Elsevier.
- Montañez, I. P., and Poulsen, C. J. (2013). The Late Paleozoic Ice Age: An Evolving Paradigm. *Annu. Rev. Earth. Planetary Sci.* 41, 629–656. doi: 10.1146/annurev.earth.031208.10118
- Montañez, I. P., McElwain, J. C., Poulsen, C. J., White, J. D., DiMichele, W. A., Wilson, J. P., et al. (2016). Climate, pCO₂ and terrestrial carbon cycle linkages during late Palaeozoic glacial–interglacial cycles. *Nat. Geosci.* 9, 824–828. doi: 10.1038/ngeo2822
- Morgan, J. (1930). *The Morphology and Anatomy of American Species of the Genus Psaronius*. Champaign: University of Illinois Press.
- Munzimi, Y. A., Hansen, M. C., Adusei, B., and Senay, G. B. (2015). Characterizing Congo Basin Rainfall and Climate Using Tropical Rainfall Measuring Mission (TRMM) Satellite Data and Limited Rain Gauge Ground Observations. *J. Appl. Meteorol. Climatol.* 54, 541–555. doi: 10.1175/JAMC-D-14-0052.1
- Nicotra, A. B., Leigh, A., Boyce, C. K., Jones, C. S., Niklas, K. J., Royer, D. L., et al. (2011). The evolution and functional significance of leaf shape in the angiosperms. *Funct. Plant Biol.* 38:535. doi: 10.1071/FP11057
- Opluštil, S., Šimůnek, Z., Zajíc, J., and Mencl, V. (2013). Climatic and biotic changes around the Carboniferous/Permian boundary recorded in the continental basins of the Czech Republic. *Int. J. Coal Geol.* 119, 114–151. doi: 10.1016/j.coal.2013.07.014
- Penman, H. L. (1948). Natural evaporation from open water, bare soil and grass. *Proc. R. Soc. Lond.* 193, 120–145. doi: 10.1098/rspa.1948.0037
- Peppe, D. J., Royer, D. L., Cariglino, B., Oliver, S. Y., Newman, S., Leight, E., et al. (2011). Sensitivity of leaf size and shape to climate: Global patterns and paleoclimatic applications. *New Phytol.* 190, 724–739. doi: 10.1111/j.1469-8137.2010.03615.x
- Pittermann, J., and Sperry, J. (2003). Tracheid diameter is the key trait determining the extent of freezing-induced embolism in conifers. *Tree Physiol.* 23, 907–914. doi: 10.1093/treephys/23.13.907
- Pittermann, J., and Sperry, J. S. (2006). Analysis of Freeze-Thaw Embolism in Conifers. The Interaction between Cavitation Pressure and Tracheid Size. *Plant Physiol.* 140, 374–382. doi: 10.1104/pp.105.067900
- Pittermann, J., Brodersen, C., and Watkins, J. E. (2013). The physiological resilience of fern sporophytes and gametophytes: Advances in water relations offer new insights into an old lineage. *Front. Plant Sci.* 4:285. doi: 10.3389/fpls.2013.00285
- Pittermann, J., Limm, E., Rico, C., and Christman, M. A. (2011). Structure-function constraints of tracheid-based xylem: A comparison of conifers and ferns. *New Phytol.* 192, 449–461. doi: 10.1111/j.1469-8137.2011.03817.x
- Pittermann, J., Sperry, J. S., Hacke, U. G., Wheeler, J. K., and Sikkema, E. H. (2006). Inter-tracheid pitting and the hydraulic efficiency of conifer wood: The role of tracheid allometry and cavitation protection. *Am. J. Bot.* 93, 1265–1273. doi: 10.3732/ajb.93.9.1265
- R Core Team, (2021). *R: A Language and Environment for Statistical Computing*. Vienna: R Foundation for Statistical Computing.
- Reynolds, F. A. (2014). *Berkshire Community College Bioscience Image Library: A Public Domain Open Educational Resource*. Available online at: <http://blogs.berkshirecc.edu/bccoer/> (accessed May 11, 2022).
- Richey, J. D. I., Montañez, P., Goddérís, Y., Looy, C. V., Griffis, N. P., and DiMichele, W. A. (2020). Influence of temporally varying weatherability on CO₂-climate coupling and ecosystem change in the late Paleozoic. *Climate Past* 16, 1759–1775. doi: 10.5194/cp-16-1759-2020
- Richey, J. D. I., Montañez, P., White, J. D., DiMichele, W. A., Matthaeus, W. J., Poulsen, C. J., et al. (2021). Modeled physiological mechanisms for observed changes in the late Paleozoic plant fossil record. *Palaeogeogr. Palaeoclimatol. Palaeoecol.* 562:110056. doi: 10.1016/j.palaeo.2020.110056
- Rico, C., Pittermann, J., Polley, H. W., Aspinwall, M. J., and Fay, P. A. (2013). The effect of subambient to elevated atmospheric CO₂ concentration on vascular function in *Helianthus annuus*: Implications for plant response to climate change. *New Phytol.* 199, 956–965. doi: 10.1111/nph.12339
- Royer, D. L. (2001). Stomatal density and stomatal index as indicators of paleoatmospheric CO₂ concentration. *Rev. Palaeobot. Palynol.* 114, 1–28. doi: 10.1016/S0034-6667(00)00074-9
- Runge, J. (2007). “The Congo River, Central Africa,” in *Large Rivers*, ed. A. Gupta (Chichester, UK: John Wiley & Sons, Ltd), 293–309. doi: 10.1002/9780470723722.ch14
- Running, S. W., and Coughlan, J. C. (1988). A general model of forest ecosystem processes for regional applications I. Hydrologic balance, canopy gas exchange and primary production processes. *Ecol. Model.* 42, 125–154. doi: 10.1016/0304-3800(88)90112-3
- Ryan, M. G. (1995). Foliar maintenance respiration of subalpine and boreal trees and shrubs in relation to nitrogen content. *Plant Cell Environ.* 18, 765–772. doi: 10.1111/j.1365-3040.1995.tb00579.x
- Sack, L., and Holbrook, N. M. (2006). LEAF HYDRAULICS. *Annu. Rev. Plant Biol.* 57, 361–381. doi: 10.1146/annurev.arplant.56.032604.144141
- Sahney, S., Benton, M. J., and Falcon-Lang, H. J. (2010). Rainforest collapse triggered Carboniferous tetrapod diversification in Euramerica. *Geology* 38, 1079–1082. doi: 10.1130/G31182.1
- Schimel, D., Melillo, J., Tian, H., McGuire, A. D., Kicklighter, D., Kittel, T., et al. (2000). Contribution of increasing CO₂ and climate to carbon storage by ecosystems in the united states. *Science* 287, 2004–2006. doi: 10.1126/science.287.5460.200
- Skelton, R. P., West, A. G., and Dawson, T. E. (2015). Predicting plant vulnerability to drought in biodiverse regions using functional traits. *Proc. Natl. Acad. Sci. U.S.A.* 112, 5744–5749. doi: 10.1073/pnas.1503376112
- Song, J., Trueba, S., Yin, X.-H., Cao, K.-F., Brodribb, T. J., and Hao, G.-Y. (2022). Hydraulic vulnerability segmentation in compound-leaved trees: Evidence from an embolism visualization technique. *Plant Physiol.* 189, 204–214. doi: 10.1093/plphys/kiac034
- Sperry, J. S., and Tyree, M. T. (1990). Water-stress-induced xylem embolism in three species of conifers. *Plant Cell Environ.* 13, 427–436. doi: 10.1111/j.1365-3040.1990.tb01319.x
- Sperry, J. S., Hacke, U. G., and Pittermann, J. (2006). Size and function in conifer tracheids and angiosperm vessels. *Am. J. Bot.* 93, 1490–1500. doi: 10.3732/ajb.93.10.1490
- Sperry, J. S., Nichols, K. L., Sullivan, J. E. M., and Eastlack, S. A. (1994). Xylem Embolism in Ring-Porous, Diffuse-Porous, and Coniferous Trees of Northern Utah and Interior Alaska. *Ecology* 75:1736. doi: 10.2307/1939633
- Sperry, J. S., Wang, Y., Wolfe, B. T., Mackay, D. S., Anderegg, W. R. L., McDowell, N. G., et al. (2016). Pragmatic hydraulic theory predicts stomatal

- responses to climatic water deficits. *New Phytol.* 212, 577–589. doi: 10.1111/nph.14059
- Steinthorsdottir, M., Jeram, A. J., and McElwain, J. C. (2011). Extremely elevated CO₂ concentrations at the Triassic/Jurassic boundary. *Palaeogeogr. Palaeoclimatol. Palaeoecol.* 308, 418–432. doi: 10.1016/j.palaeo.2011.05.050
- Suissa, J. S., and Friedman, W. E. (2021). From cells to stems: The effects of primary vascular construction on drought-induced embolism in fern rhizomes. *New Phytol.* 232, 2238–2253. doi: 10.1111/nph.17629
- Sussmilch, F. C., Brodribb, T. J., and McAdam, S. A. M. (2017). What are the evolutionary origins of stomatal responses to abscisic acid in land plants?: Evolution of stomatal responses to ABA in land plants. *J. Integr. Plant Biol.* 59, 240–260. doi: 10.1111/jipb.12523
- Tabor, N. J., DiMichele, W. A. I., Montañez, P., and Chaney, D. S. (2013). Late Paleozoic continental warming of a cold tropical basin and floristic change in western Pangea. *Int. J. Coal Geol.* 119, 177–186. doi: 10.1016/j.coal.2013.07.009
- Taylor, T. N., Taylor, E. L., and Krings, M. (2009). *Paleobotany: The Biology and Evolution of Fossil Plants*, 2nd Edn. Cambridge, MA: Academic Press.
- Thompson, S. L., and Pollard, D. (1997). Greenland and Antarctic Mass Balances for Present and Doubled Atmospheric CO₂ from the GENESIS Version-2 Global Climate Model. *J. Climate* 10, 871–900. doi: 10.1175/1520-0442(1997)010<0871:GAAMBF>2.0.CO;2
- Thonglim, A., Delzon, S., Larter, M., Karami, O., Rahimi, A., Offringa, R., et al. (2021). Intervessel pit membrane thickness best explains variation in embolism resistance amongst stems of *Arabidopsis thaliana* accessions. *Ann. Bot.* 128, 171–182. doi: 10.1093/aob/mcaal96
- Thornton, P. E., Law, B. E., Gholz, H. L., Clark, K. L., Falge, E., Ellsworth, D. S., et al. (2002). Modeling and measuring the effects of disturbance history and climate on carbon and water budgets in evergreen needleleaf forests. *Agricult. Forest Meteorol.* 113, 185–222. doi: 10.1016/S0168-1923(02)00108-9
- Thornton, P. E., and Rosenbloom, N. A. (2005). Ecosystem model spin-up: Estimating steady state conditions in a coupled terrestrial carbon and nitrogen cycle model. *Ecol. Modelling* 189, 25–48. doi: 10.1016/j.ecolmodel.2005.04.008
- Tyree, M. T., and Ewers, F. W. (1991). The hydraulic architecture of trees and other woody plants. *New Phytol.* 119, 345–360. doi: 10.1111/j.1469-8137.1991.tb00035.x
- Tyree, M. T., and Sperry, J. S. (1988). Do Woody Plants Operate Near the Point of Catastrophic Xylem Dysfunction Caused by Dynamic Water Stress?: Answers from a Model. *Plant Physiol.* 88, 574–580. doi: 10.1104/pp.88.3.574
- Tyree, M. T., and Sperry, J. S. (1989). Vulnerability of Xylem to Cavitation and Embolism. *Annu. Rev. Plant Physiol. Plant Mol. Biol.* 20, 19–36. doi: 10.1146/annurev.pp.40.060189.000315
- Tyree, M. T., and Zimmermann, M. H. (2002). *Xylem Structure and the Ascent of Sap*, 2nd Edn. Berlin: Springer. doi: 10.1007/978-3-662-04931-0
- Utsumi, Y., Sano, Y., Funada, R., Ohtani, J., and Fujikawa, S. (2003). Seasonal and Perennial Changes in the Distribution of Water in the Sapwood of Conifers in a Sub-Frigid Zone. *Plant Physiol.* 131, 1826–1833. doi: 10.1104/pp.102.014795
- Venturas, M. D., Sperry, J. S., and Hacke, U. G. (2017). Plant xylem hydraulics: What we understand, current research, and future challenges. *J. Integrat. Plant Biol.* 59, 356–389. doi: 10.1111/jipb.12534
- Viney, M., Hickey, R. D., and Mustoe, G. E. (2019). A Silicified Carboniferous Lycopodioid Forest in the Colorado Rocky Mountains, USA. *Geosciences* 9:510. doi: 10.3390/geosciences9120510
- Wagner, F., Aaby, B., and Visscher, H. (2002). Rapid atmospheric CO₂ changes associated with the 8,200-years-B.P. cooling event. *Proc. Nat. Acad. Sci. U.S.A.* 99, 12011–12014. doi: 10.1073/pnas.182420699
- Watkins, J. E., Holbrook, N. M., and Zwieniecki, M. A. (2010). Hydraulic properties of fern sporophytes: Consequences for ecological and evolutionary diversification. *Am. J. Bot.* 97, 2007–2019. doi: 10.3732/ajb.1000124
- Wheeler, J. K., Sperry, J. S., Hacke, U. G., and Hoang, N. (2005). Inter-vessel pitting and cavitation in woody Rosaceae and other vesselless plants: A basis for a safety versus efficiency trade-off in xylem transport. *Plant Cell Environ.* 28, 800–812. doi: 10.1111/j.1365-3040.2005.01330.x
- White, D. A. (1992). Relationships between foliar number and the cross-sectional areas of sapwood and annual rings in red oak (*Quercus rubra*) crowns. *Canad. J. Forest Res.* 23, 1245–1251. doi: 10.1139/x93-159
- White, J. D. I., Montañez, P., Wilson, J. P., McElwain, J. C., DiMichele, W. A., Hren, M. T., et al. (2020). A Process-Based Ecosystem Model (Paleo-BGC) to Simulate the Dynamic Response of Late Carboniferous Plants to Elevated O₂ And Aridification. *Am. J. Sci.* 320, 547–598. doi: 10.2475/09.2020.01
- White, M. A., Thornton, P. E., Running, S. W., and Nemani, R. R. (2000). Parameterization and Sensitivity Analysis of the BIOME-BGC Terrestrial Ecosystem Model: Net Primary Production Controls. *Earth Interactions* 4, 1–85. doi: 10.1175/1087-3562(2000)004<0003:PASAOT>2.0.CO;2
- White, R. A. (1962). *A Comparative Study of the Tracheary Elements of the Ferns*, Ph.D thesis. Arbor, MI: University of Michigan.
- Willis, C. G., Baskin, C. C., Baskin, J. M., Auld, J. R., Venable, D. L., Cavender-Bares, J., et al. (2014). The evolution of seed dormancy: Environmental cues, evolutionary hubs, and diversification of the seed plants. *New Phytol.* 203, 300–309. doi: 10.1111/nph.12782
- Wilson, J. P. (2013). Modeling 400 Million Years of Plant Hydraulics. *Paleontol. Soc. Papers* 19, 175–194. doi: 10.1017/S1089332600002734
- Wilson, J. P. (2016). Hydraulics of Psilophyton and evolutionary trends in plant water transport after terrestrialization. *Rev. Palaeobot. Palynol.* 227, 65–76. doi: 10.1016/j.revpalbo.2015.11.010
- Wilson, J. P. I., Montañez, P., White, J. D., DiMichele, W. A., McElwain, J. C., Poulsen, C. J., et al. (2017). Dynamic Carboniferous tropical forests: New views of plant function and potential for physiological forcing of climate. *New Phytol.* 215, 1333–1353. doi: 10.1111/nph.14700
- Wilson, J. P., and Fischer, W. W. (2011). Hydraulics of *Asteroxylon mackei*, an early Devonian vascular plant, and the early evolution of water transport tissue in terrestrial plants. *Geobiology* 9, 121–130. doi: 10.1111/j.1472-4669.2010.00269.x
- Wilson, J. P., and Knoll, A. H. (2010). A physiologically explicit morphospace for tracheid-based water transport in modern and extinct seed plants. *Paleobiology* 36, 335–355. doi: 10.1666/08071.1
- Wilson, J. P., Knoll, A. H., Holbrook, N. M., and Marshall, C. R. (2008). Modeling fluid flow in *Medullosa*, an anatomically unusual Carboniferous seed plant. *Paleobiology* 34, 472–493. doi: 10.1666/07076.1
- Wilson, J. P., White, J. D. I., Montañez, P., DiMichele, W. A., McElwain, J. C., Poulsen, C. J., et al. (2020). Carboniferous plant physiology breaks the mold. *New Phytol.* 227, 667–679. doi: 10.1111/nph.16460
- Wilson, J. P., White, J. D., DiMichele, W. A., Hren, M. T., Poulsen, C. J., McElwain, J. C., et al. (2015). Reconstructing Extinct Plant Water Use for Understanding Vegetation–Climate Feedbacks: Methods, Synthesis, and a Case Study Using the Paleozoic-Era *Medullosa* Seed Ferns. *Paleontol. Soc. Papers* 21, 167–196. doi: 10.1017/S1089332600003004
- Woodward, F. I. (1987). Stomatal numbers are sensitive to increases in CO₂ from pre-industrial levels. *Nature* 327, 617–618. doi: 10.1038/327617a0
- Yang, S., and Tyree, M. T. (1992). A theoretical model of hydraulic conductivity recovery from embolism with comparison to experimental data on *Acer saccharum*. *Plant Cell Environ.* 15, 633–643. doi: 10.1111/j.1365-3040.1992.tb01005.x
- Yin, J., Fridley, J. D., Smith, M. S., and Bauerle, T. L. (2016). Xylem vessel traits predict the leaf phenology of native and non-native understorey species of temperate deciduous forests. *Funct. Ecol.* 30, 206–214. doi: 10.1111/1365-2435.12476
- Zeppel, M., and Eamus, D. (2008). Coordination of leaf area, sapwood area and canopy conductance leads to species convergence of tree water use in a remnant evergreen woodland. *Aust. J. Bot.* 56:97. doi: 10.1071/BT07091
- Zimmermann, M. H., McCue, K. F., and Sperry, J. S. (1982). Anatomy of the Palm *Rhapis excelsa*, VIII Vessel Network and Vessel-Length Distribution in the Stem. *J. Arnold Arboretum.* 63, 83–95. doi: 10.5962/p.247644